Adsorpcja i samoorganizacja molekuł organicznych na bogatej w ind powierzchni InSb(001) – modelowanie metodami funkcjonału gęstości

Dawid Toton

Rozprawa doktorska

Promotor:

Prof. Marek Szymoński

Kopromotor:

Prof. Lev Kantorovich

Uniwersytet Jagielloński
Instytut Fizyki im. Mariana Smoluchowskiego
Zakład Fizyki Nanostruktur i Nanotechnologii

Kraków, 2012

Density functional theory study of adsorption and self-assembly of organic molecules on the indium-rich InSb(001) surface

Dawid Toton

Ph. D. thesis under supervision of
Prof. Marek Szymoński
Co-supervisor:
Prof. Lev Kantorovich

Jagiellonian University
Institute of Physics
Department of Physics of Nanostructures and Nanotechnology

Kraków, 2012

Introduction

Technology development strives for construction of possibly small and fast devices. Thus, future electronics is expected to be realized at the nanoscale. Specifically designed and synthesized molecules will act as individual functional units [1].

With this end in view, the following two aspects need to be considered: precise control of large number of such elements constituting a macro-scale device, and mastery of structures at the atomic level. Research on the latter problem was revolutionized by advent of the scanning probe microscopy. Direct manipulation of single atoms was made possible.

Flat and clean crystal surfaces have become an arena of these experiments. Two- and one-dimensional structures are grown and examined, but also local phenomena, such as defects and interaction with individual atoms or molecules are observed. Before more complex systems are developed, properties of their anticipated constituents is investigated.

In particular, a well-known organic semiconductor molecule PTCDA has been extensively studied on many substrates. Among them is the (001)

1

surface of indium antimonide. The surface has very complex structure, as it is common for compound semiconductors. It was a subject of many studies and there were several models of it proposed. The work presented in this dissertation advances its understanding further and, at the same time, solves the problem of adsorption and conformations of PTCDA molecule on this surface. This is achieved by means of DFT calculations.

Their outcome proved entirely consistent with results of experiments conducted in parallel to the research presented here. It exemplifies the great help coming from coordination of theoretical and experimental efforts.

Acknowledgements

I wish to express my gratitude to my Ph.D. supervisor, prof. dr hab. Marek Szymoński, for all the time and assistance he generously offered me throughout my Ph.D. studies. I also greatly appreciate the help of professor Lev Kantorovich, a co-supervisor, whose expertise and very friendly support made this research possible. In particular, I am very grateful for multiple opportunities to visit him and work with his group. It is also difficult to overstate the importance of his efforts to make the essential computational resources available.

Finally, I would like to thank all the people whose help and discussions contributed to this research.

Contents

List of Figures

7

List of Tables

Chapter 1

Computational methods

Computer simulation of physical phenomena can be seen as a replacement for experiments or as a tool that complements them. When it is considered as an *in silico* experiment itself, it can not only reveal the final outcome, but also brings a possibility to look inside, to understand causes of the identified behaviour that are not directly observable. Thus, for example, if we predict infra-red spectrum of a molecule by theoretical calculation, not only vibrational spectra are delivered but also a detailed insight into individual vibrational modes is gained.

Broad range of problems in solid state physics and chemistry can be addressed this way. They are well represented by a simple model. It consists of possibly infinite set of atoms. Each nucleus and each electron moves in electrostatic potential of all other particles. Some problems require interaction with an external field to be included. As the core parts of the heaviest

atoms can be approximately represented by a pseudopotential, so that the innermost electrons do not appear explicitly in the calculations, it is possible to avoid explicit relativistic treatment.

This simple model, a description of interacting electrons and nuclei, covers much of our reality down to the nanometre scale. Its application is limited only by available computational power.

The frequently used term *ab initio* describes a calculation done purely from first principles, namely the Schrödinger equation together with Hamiltonian of particles bound by Coulomb interaction. The same can be said in case of the the work presented here, although to some extent, usage of pseudopotentials, which are tuned for specific applications, encumbers the method by some dependence on experimental data.

1.1 General statement of the considered problem

Since atomic nuclei are much heavier than electrons, their dynamics can be treated separately. State of the electrons can be found with good accuracy if the nuclei are assumed to stay at rest. This is so-called Born-Oppenheimer approximation. With help of it, energetics of the whole system is studied at two levels. The core many-body problem involves electrons only and is solved for a given potential V, which is the field of all nuclei. On top of this solution, the classical behaviour of nuclei is easily described, leading to the

notion of energy surface discussed below.

Hence, at first we are given coordinates R_i of atomic nuclei, leading to a particular potential V. It suffices to solve stationary Schrödinger equation,

$$H\psi = E\psi \tag{1.1}$$

for a spectrum of energies E_i and states ψ_i. The Hamiltonian contains kinetic energy term and Coulombic interactions (for clarity, atomic units are used):

$$H = -\frac{1}{2}\sum_i \nabla_{r_i}^2 + \sum_i V(r_i) + \sum_{i<j} \frac{1}{|r_i - r_j|} \tag{1.2}$$

In practice, most often only the ground state ψ_0 is needed and it is the easiest one to obtain. Closer examination of the calculated wavefuction permits discussion of issues such as chemical binding [6], localization of charges, vacuum states, etc.

Usually the electronic problem is solved many times for many configurations of nuclei. This makes possible to find the optimal arrangement of atoms in the simulated system, examine its vibrational properties, find metastable configurations, discover paths of chemical reactions, etc. This is most conveniently discussed with the notion of energy surface.

1.2 The energy surface

Consider an investigation of dynamics of the whole system, in which number M of atoms in the system remains constant. The positions $R_1, \ldots, R_M$ of nuclei are varied and the system is solved for ground state. The ground state energy $E(R_1, \ldots, R_M)$ as a function of these positions is called an energy surface.

Since its domain has many dimensions, it is possible to explore only tiny part of it and its typical depictions are in fact only two or three-dimensional cross-sections.

It is natural to seek for a guidance in this vast space, to follow only the most important directions. In our case the coordinates of crucial significance are the positions of atoms that belong to the PTCDA molecule. Since we want to control the translational component of its movement, it suffices to pay attention to only one atom. For the diffusion study, described in section 3.7, one of the innermost carbon atoms of the perylene core was chosen.

1.3 Optimization

Although only finite, non-zero temperatures are realized in nature, finding the state corresponding to absolute zero is often enough for understanding of the system at its equilibrium. This state is found where the energy surface has its global minimum.

For this, two tasks can be distinguished. First, to discover which of all

the minima (which can be numerous) is the deepest one. In other words, to find its basin in the phase space. The second problem concerns precise location of the minimum.

Function optimization, in both of these aspects, is a very general and universally applicable concept. However, only some of the great number of developed methods are applicable for the specific case of atomic simulations.

Number of atoms in currently attainable DFT-level calculations reaches the order of thousands. Optimization of atomic positions with this number of degrees of freedom can be considered as medium-sized problem. The explored energy surface is continuous. Evaluation of each point is costly, but the numerical noise of the results is usually so small, that it does not influence choice of the optimization algorithm.

While for typically sized problems exhaustive search in the whole phase space is impossible, satisfactory solutions can be obtained thanks to advantageous properties of the energy surface. Namely, it appears as if it was a sum of simpler functions, so that the deepest basins make the surrounding local minima lower. Also, in the same way, the right direction of search can be found following low-energy barrier crossings [7].

Of the two problems mentioned above, the second one, namely, local optimization of energy, is much simpler. Since the examined function is smooth, it is usually modelled by a truncated Taylor expansion. A minimum of the model itself is easily found. As the expansion coefficients are refined, the model minimum comes closer to the true optimal point. The assumed

model often serves only as a justification of a simpler, one-dimensional model built along carefully chosen series of directions.

In particular, if optimization proceeds along gradient vectors found at each of the examined points (the so-called steepest descent algorithm), the convergence can be slow. Much better results are achieved if one makes use of second derivatives (the Hessian matrix) of the objective function. However, since matrix inversion is a costly operation, approximations are used. For example, one of methods, that are important in the context of atomic-scale calculations, is the limited-memory version of Broyden–Fletcher–Goldfarb–Shanno scheme[8]. It makes use of few gradient vectors available from the most recent steps to estimate local curvature of the optimized function.

Another widely used method, the method of conjugate gradients [9] is based on the idea that subsequent one-dimensional searches should be independent. The formula is derived to lead to the exact solution in N steps for N-dimensional domain in an idealized case of quadratic function. Still, it is reformulated and used to solve other nonlinear problems for which the assumed model is reasonable.

Because of the above-mentioned sum-like appearance of the objective function, global optimization can be helped if the function is smoothed. This can be done by averaging the slope observed along the search path. In this case it is said that a momentum is introduced into the scheme. In the context of chemistry and physics simple optimization methods with gradient averaging are often called damped molecular dynamics. If the idea is paired with

clever heuristics, the resulting algorithm can deal with both local and global optimization problems [10]. This property makes it very convenient to be used to work with atomic structures.

In the cases when the optimized function is poorly understood, one turns to stochastic optimization. It means that the choice of sampling points in the search space is in large part randomized. For the work presented here the most relevant method of this sort is the so-called simulated annealing [11]. It can be realized as a molecular dynamics with continuously lowered temperature.

1.4   Search for a transition path

It is often desirable to predict theoretically what evolution of state of a system can lead from one energy well (basin of a minimum) to another. Given two extreme states, it is possible to find a path connecting them with locally minimal free energy – the most likely transition sought for.

The most straightforward solution is to start with an initial guess of the path, for example a straight line in the phase space, and then optimize it to meet the desired criteria. It is convenient to represent the path as a series of points. Then a vibrational analysis or simple molecular dynamic helps to determine the entropic contribution at each point. Optimization of free energy leads to movements of these points across the path. The above ideas are the basis of a family of the so-called elastic band methods and many

other algorithms that find transition states [12].

1.4.1   Search by simple constrained minimization

If less accurate results are acceptable, a much simpler scheme is of use. Namely, the path can be built point by point, starting from a chosen end state. Steady progress of this procedure is enforced by constraining subsequent points so that their projections to a line which joins the extreme states are at equal distances. A simpler projection of similar properties can be used as well. For each added point local minimum serves as a best guess. This is not always the right choice, as demonstrated on Fig. 1.1. The picture shows an example of energy surface and two transition paths: as obtained by the procedure described here (a) and the optimal one (b). A sudden transition to another energy basin along the dashed line manifests itself as a discontinuity in the energy. Thus, in general, the energy barriers discovered with this method are possibly overestimated.

1.5   Overview of the methods to solve the problem of many electrons

Now we return to the problem of many electrons. The first striking property of our task is its high dimensionality. We wish to deliver a wavefunction as an output of the most important first stage of the calculation. Alas, this function
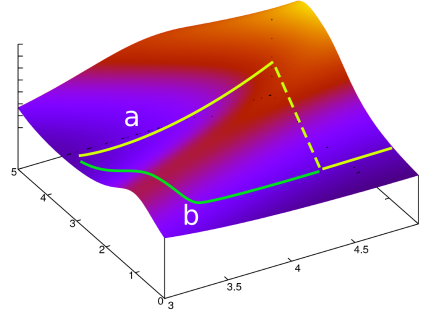
Figure 1.1: An example of energy surface for which the energy barrier found by series of constrained optimizations is too high. The path found by this method (a) and the optimal path (b) are shown.

ψ, which carries complete description of state of N electrons, is a $\mathbb{R}^{3N} \to \mathbb{C}$ function. So for relatively small count of electrons $N = 100$ and for any naive sampling of some finite region of the real space, the function cannot be directly represented in any imaginable volume of computer hardware. Therefore ψ has to be encoded in a compact way and in practice it has also to be approximated. This is done with great success with the family of methods called Quantum Monte-Carlo [13]. Among them the Diffusion Monte Carlo [14, 15, 16] is based on a very fortunate coincidence, namely that the evolution steps of wavefunction that are dictated by imaginary-time Schrödinger equation can be directly performed on a Monte-Carlo-friendly representation of the wavefunction, that is, a set of points in $\mathbb{R}^{3N}$ space.

Very compact and computationally cheap representations of the wave-function can be chosen if significant approximations are to be made from start. First of all, one can consider only the simplest antisymmetric states,

namely, Slater determinants. One can look for the state of lowest energy in this convenient space. This method is called Hartree-Fock [17, 18]. As an aside, it is interesting to note that the density functional theory in the Kohn-Sham formulation discussed in section 1.5.2 works in the same space, but different condition is imposed on the solution chosen, so eventually a different state is selected. The Hartree-Fock method is a first member of a broader family of algorithms. If the explored space consists of states built from many Slater determinants, the methods are called Configuration Interaction [19].

The Coupled-Cluster methods [20, 21], which deliver results of very high accuracy, can also be seen as derived from Hartree-Fock. In this case the state is represented as $e^T \phi$, where ϕ is a simple Slater state and the exponentiation e^T captures infinitely many excitations (or, in practice, as many as the chosen basis permits). The coefficients constructing the operator T are what the methods finds.

Alternatively, we can give up dealing with the highly dimensional space containing ψ and seek for other quantity, derived from ψ, that would serve our particular goals as well.

Intuitively, since the computed many-body wavefunction is antisymmetric with respect to exchange of electrons, very little should be lost when its domain is reduced by some kind of integration. It turns out that such reduction is useful if done to the density matrices.

Our model involves only two-body interactions, so, in fact, we can get rid of nearly all of the dimensions and still have an exact expression of E in terms of quantities derived from the wavefunction ψ. Two-particle density matrix in a basis of position is a $\mathbb{R}^{12} \to \mathbb{C}$ function[22]:

$$\Gamma(r_1, r_2, R_1, R_2) =$$

$$N(N-1) \int dp_3 ... \int dp_N \psi^*(r_1, r_2, p_3, ..., p_N) \psi(R_1, R_2, p_3, ..., p_N) \qquad (1.3)$$

The one-particle density matrix

$$\gamma(r, R) = N \int dp_2 ... \int dp_N \psi^*(r, p_2, ..., p_N) \psi(R, p_2, ..., p_N) \qquad (1.4)$$

can be expressed as $\gamma(r, R) = \frac{1}{N-1} \int dp_2 \Gamma(r, p_2, R, p_2)$ and also particle density is

$$n(r) = N \int dp_2 ... \int dp_N \psi^*(r, p_2, ..., p_N) \psi(r, p_2, ..., p_N) = \gamma(r, r) \qquad (1.5)$$

The energy then becomes [22]

$$E = -\frac{1}{2} \int dr \nabla_R^2 \gamma(r, R)|_{R=r} + \int dr V(r) n(r) + \frac{1}{2} \int dr_1 \int dr_2 \frac{\Gamma(r_1, r_2, r_1, r_2)}{|R - r|} \qquad (1.6)$$

This allows us to employ variational methods working in an approachable space of $\mathbb{R}^{12} \to \mathbb{C}$ functions. A first impression may be that this should lead to a computationally feasible method solving our many-body problem

exactly. But, surprisingly, the whole complexity lies hidden in the indispensable condition, that the outcome Γ has to correspond to some normalized N-body wavefunction [23]. Nevertheless, these methods, labelled 2-RDM (meaning two-particle reduced density matrix), provide high quality results even if the representability condition is not exactly satisfied [24].

If the above-mentioned dimensionality reduction is carried a little further, the search can be performed in even smaller space, but the results are no longer conceptually exact. The Density Matrix Functional Theory assumes γ as a basic variable. In this case the electron-electron interaction term in equation 1.6 can rely only on approximation of $\Gamma(\gamma)$, which becomes a function of γ. Practically useful approximations contain corrections expressed in terms of natural orbitals ϕ of γ. For example, a starting point given by Müller [25] and later by Buijse and Baerends [26]:

$$\Gamma_{BB}(r_1, r_2) = n(r_1)n(r_2) - \sum_{ij} \sqrt{\mu_i \mu_j}\phi_i^*(r_1)\phi_j(r_1)\phi_i(r_2)\phi_j^*(r_2) \qquad (1.7)$$

where μ denote occupancies of the orbitals. The approximation is then refined by adding more correction terms.

Finally, if just the particle density $n(r)$ is used as the basic quantity, exact kinetic energy becomes no longer available and a framework called Density Functional Theory emerges.

1.5.1 Density Functional Theory

Let S denote basis of space of states of a single electron. Then, states of N electrons belong sto the antisymmetric portion of the space spanned by S^N. For example, points in real space with spin can serve this purpose: $S = \mathbb{R}^3 \times \{\uparrow, \downarrow\}$. For brevity, coordinates in the following discussion are from S, that is, $r_i \in S$. The expression $|r1 - r2|$, a particle-particle distance, will accordingly refer to a norm in S which ignores the spin dimension.

As explained below, working only with electron densities

$$n_\psi(r) = N \int dr_2 \ldots \int dr_n \psi^*(r, r_2, \ldots, r_n) \psi(r, r_2, \ldots, r_n) \qquad (1.8)$$

it is possible to find some description of the ground state: its energy E_0 and the corresponding density $n_0(r)$. To be precise, Kohn-Sham methods, as described later, use auxiliary orbitals and thus go beyond the simple idea of calculation based on density only. This is especially visible in case of the most elaborate approximations, in which the orbitals serve calculation of exact exchange energy. Still, the density $n(r)$ retains its central position at the conceptual level.

The looked-for density n_0 corresponds to the state ψ_0 of the lowest energy. It can be found by optimization of energy expressed as a function of n (called a *functional* as the density n itself is a function and $E \in \mathbb{R}^{R^S}$ with some

$R \subset \mathbb{R}$) in the following way [27]:

$$E(n) = \min_{\psi: n_\psi = n} \langle \psi | H | \psi \rangle \tag{1.9}$$

Obviously, direct Rayleigh-Ritz variational procedure and the two stage optimization described above both explore the whole space of antisymmetric N-particle wavefunctions and come to the same ground state energy E_0:

$$E_0 = E(n_0) = \langle \psi_0 | H | \psi_0 \rangle \tag{1.10}$$

Hence, the ground state density and energy can be found at minimum of the functional $E(n)$. This result is known as the second Hohenberg-Kohn theorem [28].

For further discussion of properties of $E(n)$, the following form of the Hamiltonian H will be assumed:

$$H = T + U + V \tag{1.11}$$

where T is the kinetic energy operator, U is electron-electron interaction and V is some local multiplicative potential. Together with boundary conditions and assumed number of particles $\int dr n(r) = N$ the potential V provides complete description of the problem to be solved. V is a one-particle operator

diagonal in real space, hence:

$$\langle\psi|H|\psi\rangle = \langle\psi|T + U|\psi\rangle + \int drn(r)V(r) \qquad (1.12)$$

Given a particular potential V, the density n_0^V that yields the optimal energy $E(n_0^V)$, always changes as the potential V is altered in a non-trivial way. This is obvious in the typical case when V is generated by atomic nuclei and the change of V is a result of their movement. Since the potential diverges at their locations, the ground state wavefunction and its density have cusps there [29]. Nevertheless, the claim can be rigorously justified as follows.

For given state ψ, the term $\langle\psi|T + U|\psi\rangle$ of the equation 1.12 does not change with V. The rest of the energy depends on V in the same way for all states which share the same corresponding electron density.

Let $\Delta E(\psi)$ denote change of energy of given state ψ as the term ΔV is introduced:

$$\Delta E(\psi) = \langle\psi|T + U + V + \Delta V|\psi\rangle - \langle\psi|T + U + V|\psi\rangle = \int drn_\psi(r)\Delta V(r)$$
$$(1.13)$$

It is crucial here that these changes depend only on electron densities instead of the full wavefuction ψ.

Nontrivial changes $\Delta V(r) \neq const$ inevitably mix[1] the ground state ψ_0^V

---

[1]Suppose that the ground state remains unchanged after ΔV is added to the potential, namely $\psi_0^V = \psi_0^{V+\Delta V}$. Energy change ΔE is an eigenvalue of potential change: $\Delta H\psi_0^V =$

with some excited states ψ_i^V and the pure ψ_0^V remains no longer of the lowest energy with the new Hamiltonian $T + U + V + \Delta V$. Thus, energy of this state grows more than energy of some mixed state $\psi_0^{V+\Delta V}$ as the potential V is changed:

$$\Delta E(\psi_0^V) > \Delta E(\psi_0^{V+\Delta V}) \tag{1.14}$$

The system finds a new electron density so that the above inequality holds:

$$\int dr n_0^V(r) \Delta V(r) > \int dr n_0^{V+\Delta V}(r) \Delta V(r) \tag{1.15}$$

It means that the new ground state has different electron density. Hence the mapping of classes of equivalent external potentials V to the corresponding ground state densities n_0^V is bijective. This observation, known as the first Hohenberg-Kohn theorem [28], was one of most important steps in development of density functional theory. Densities contained in codomain of this mapping are called v-representable. Intuitively, the theorem shows that these densities contain as much information as the corresponding wavefunctions ψ.

Curiously, while density functional theory has its roots in the above considerations, in fact, its success doesn't depend on them being correct. The practically attainable approximations do not require the underlying functional to be precisely correct nor to lead to the true ground state. Moreover, routinely employed non-local pseudopotentials violate the basic assumption

---

$\Delta E \psi_0^V$. Since ΔV is diagonal in real space and at the same time ψ is its eigenvector, it must be degenerate: $\Delta V(r) = const$.

about locality of the external potential V, which is probably inescapable [30] in the above reasoning. Still the DFT methods are successful.

Having the considered particular form of the Hamiltonian in mind, the previously defined function $E(n)$ can be expressed as a sum:

$$E(n) = \min_{\psi:n_\psi=n} \langle\psi|T + U + V|\psi\rangle = \min_{\psi:n_\psi=n} \langle\psi|T + U|\psi\rangle + \int drn(r)V(r)$$

(1.16)

The first term doesn't depend on V and thus it is universal. It is called the Hohenber-Kohn functional:

$$F(n) = \min_{\psi:n_\psi=n} \langle\psi|T + U|\psi\rangle$$

(1.17)

Clearly, this leads to a simple recipe solving the problem of N electrons in the potential v: once F is known, it suffices to minimize $E(n) = F(n) + \int drn(r)V(r)$ as expressed in equation 1.16 in the space of densities n which correspond to a N-body wavefunction. In general, such condition is called N-representability. In case of the one-particle density n, it reduces just to a norm constraint [31]:

$$\int drn(r) = N$$

(1.18)

The functional F encapsulates all the complexity of the many-body problem, hence its natural that no closed form of it was found. Several families of its aproximations were developed, but none of them admits a way of systematic accuracy improvement.

1.5.2 Kohn-Sham method

It is possible to have an approximation of F based directly on the density n. This leads to the so-called orbital-free approach [32]. More accurate results are achieved if an auxiliary system of noninteracting particles is employed. This method, named after Kohn and Sham, is the more popular way followed in practical implementations. It addresses the difficulty of estimation of kinetic energy term of F. The idea is to define the auxiliary system to exactly reproduce the true electronic density and energy, making its state somewhat similar to the solution. Consequently, it is possible to capture large portion of the energy in few simple terms. The auxiliary Hamiltonian $T + V_{eff}$ lacks the usual electron-electron repulsion term. Instead, the effective potential V_{eff} is changed as the density n changes and this dependence is laboriously tuned to reproduce many-body effects.

This auxilary problem contains only one-particle operators, so a simple Slater determinant $|\phi\rangle$ solves it. Hence given the right V_{eff}, it suffices to diagonalize the effective Hamiltonian using one of many well established methods, in order to obtain the orbitals of ϕ and the energy $\langle\phi|T + V_{eff}|\phi\rangle$. Because of mutual dependency of V_{eff} and n, a consistent solution needs to be found iteratively. Extrapolation techniques, such as DIIS [33], are used for good convergence.

The auxiliary solution $|\phi\rangle$ is a function of electron density n. It is used as a tool to decompose the true energy $F(n)$, as shown below.

First, define the correlation energy

$$E_c(n) = F(n) - \langle \phi(n)|T + U|\phi(n)\rangle \qquad (1.19)$$

which is the energy released by relaxation of $|\phi\rangle$ to the true ground state $|\psi\rangle$. It is the main quantity for which complicated approximations are employed.

In addition to this, calculations of $F(n)$ require determination of $\langle \phi(n)|T|\phi(n)\rangle$, which is easy, and $\langle \phi(n)|U|\phi(n)\rangle$.

As $\phi(n)$ is a determinant state, evaluation of $\langle \phi(n)|U|\phi(n)\rangle$ is costly, so in practice often the pure Hartree repulsion

$$U_H(n) = \frac{1}{2}\int dr_1 \int dr_2 \frac{n(r_1)n(r_2)}{|r_1 - r_2|} \qquad (1.20)$$

is used as a base for another approximation, that is, the exchange energy $E_x(n)$ defined as

$$\langle \phi(n)|U|\phi(n)\rangle = U_H(n) + E_x(n) \qquad (1.21)$$

has to be expressed in terms of electon density as accurately as possible.

In summary, the energy is calculated as follows:

$$F(n) = T_\phi(n) + (U_H(n) + E_x(n)) + E_c(n) = T_\phi(n) + U_H(n) + E_{xc}(n) \quad (1.22)$$

The last term is called exchange-correlation energy. Luckily, in case of the basic density functionals, errors in E_x and E_c tend to cancel each other

for valence electrons [34].

1.5.3   Approximate functionals

Useful approximations of E_{xc} are found after a general form is imposed, as implied by loosely assumed computational costs. This could be for example integration of semi-local contributions all over the space:

$$F(n) = \int dr f\left(n(r), \Delta n(r)\right) \tag{1.23}$$

Then, limits with known behaviour are chosen to be obeyed. The functional can be fitted to accurate Quantum Monte-Carlo calculations and tuned to a set of benchmark tests (like, for example, large number of molecules).

As said, the densities n are defined in space-spin coordinates. They consist of $n_\uparrow$ and $n_\downarrow$ components, thus allowing studies of magnetic effects. Even if they are of no interest, keeping the components separate leads to better results than with single spinless electron density.

The simplest recipe for E_{xc} that was widely applied is called Local Density Approximation: $F(n) = \int dx f(n_\uparrow(x) + n_\downarrow(x))$, where x is a space coordinate. It assumes that at each point in space electrons can be treated as homogeneous gas. A version generalized to a spin-dependent form $F(n) = \int dr f(n(r))$ (note that r is a space-spin coordinate) is called Local Spin Density Approximation [35].

Many analytical forms of it were developed, such as a functional by

Perdew and Wang [36]. This approximation works well for solid-state calculations but its description of molecules is worse [34].

All calculations in this work were performed using the so-called generalized gradient approximation (GGA), which has wider applicability. The commonly used parametrisation found by Perdew, Burke and Ernzerhoff [37] was used.

The GGA permits the energy to depend on density gradient:

$$E_{xc}(n_\uparrow, n_\downarrow) = \int dr f(n_\uparrow, n_\downarrow, \nabla n_\uparrow, \nabla n_\downarrow) \tag{1.24}$$

The PBE approximation was built specifically to obey many correct scaling relations: limits of slowly varying density, rapid variations and high density, also spin-scalinig property of exchange energy and the Lieb-Oxford bound [37].

Inclusion of the density gradient results in important enhancement of description of electronic behaviour far from nuclei. It corrects the tendency of LDA to bind too strongly.

More accurate exchange-correlation functionals are classified as meta-GGAs (making use of local kinetic energy or density Laplacian), hyper-GGAs (that rely on exact exchange energy) and methods using the unoccupied Kohn-Sham orbitals. The so-called hybrid functionals mix some of the exact exchange energy into ordinary GGAs. As the DFT methods were generalized and extended, many more schemes were developed to address particular

concerns like correlation in Mott insulators and inclusion of van der Waals forces.

1.6   Treatment of infinite-sized systems

Among many interesting infinitely extended systems imaginable, only translationally symmetric ones can be practically treated by the available DFT tools. In other words, *periodic boundary conditions* are commonly imposed. They are defined by lattice vectors together with content of the unit cell.

As all effects of electron-electron interaction and also the exchange energy is encompassed by the density functional, hiding many-body nature and antisymmetricity of the wavefunction, a problem of single particle in effective potential eventually remains to be solved. In case of periodic system, the single-particle solutions obey the Bloch theorem. Namely, a plane wave e^{ikr} can be factored out of the solution, so the remaining factor has the same periodicity as the potential. The solutions are therefore arranged in groups indexed by the vector k, which belongs to the first Brillouin zone. It can be assumed that they change continuously with k. Hence the computational effort need not to be infinite – thanks to interpolation or even simple summation only few k-points are needed to integrate over all the Brillouin zone.

For calculations performed in this work the Monkhorst-Pack [38] selection of k-points is used – a regular grid in the reciprocal space. In all cases the periodic boundary conditions were imposed. Single molecule on an in-

finite surface was approximated by an infinite array of molecules placed on supercells (multiple surface reconstruction cells) chosen big enough to keep interaction between the molecules negligible.

In fact, only a portion of these k-points is retained in accordance with the expected dimensionality of the relevant part of the Brillouin zone. The vacuum region between model surface slabs reduces it to a plane. In the extreme case of isolated molecules, only $k = 0$ (denoted Γ) is kept.

1.7   Simulation of Scanning Tunneling Microscopy

The nanoscale systems studied in this work are most commonly observed with scanning probe microscopy (SPM). In particular, the scanning tunnelling microscopy (STM) provides insight into electronic details in real space.

High spatial resolutions are possible thanks to the fact that the current tunnelling through the vacuum region separating the probe and a sample decays exponentially with increase of the distance [39]. In the most often used mode of its operation, the constant current mode, height of the tip is continuously adjusted to drive the current to a constant prescribed value. Typical values of the current are from pico- to nanoampers. Maps of height as a function of probe position are subject to interpretation.

In order to simulate STM action, the tunnelling current needs to be calculated. A very simple approximation of it was derived by Tersoff and Hamann [40]. It comes from the expression obtained by Bardeen for a tunnel junction

[41], after small bias voltage and zero temperature is assumed and the probe tip is represented by a spherically-symmetric potential. The model reduces so that the tip can be considered as perfectly localized and, finally, the current is proportional to local density of states of the sample at Fermi level that would be found where the centre of the tip is located:

$$I \sim U \int_i |\psi_i(r_0)|^2 \, \delta(E_i - E_F)$$

Here ψ_i are single-electron states of energies E_i and r_0 is the tip centre.

For approximate treatment of nonzero bias voltages U the formalism is extended by summation (or integration) of densities of more orbitals as dictated by the model employed by Bardeen:

$$I \sim \sum_{i: E_F < E_i < E_F + eU} |\psi_i(r_0)|^2$$

where the condition for domain of summation should be reversed for negative U.

In principle, it is impossible to find the tunnelling current with help of DFT calculation since it delivers only the ground state electron density and energy. However, it was found that if the auxiliary non-interacting Kohn-Sham orbitals are used to derive other quantities, as if they were the ground state, useful results are obtained. Hence, throughout this work this approximation is used for modelling of STM.

In this scheme, it suffices to find an isosurface of the integrated local density of states in order to simulate an STM microscope working in the constant current mode. However, the proportionality constant, even in the simplest Tersoff-Hamann model, cannot be predicted, because it depends on the tip radius, decay constant of the assumed s-type orbital and work function of the tip and substrate. Therefore, the density values used for STM simulation are chosen to correspond to reasonable probe-surface distances. In case of calculations with localized orbitals, the distance is limited by range of these orbitals. An effect of such a local deficiency of the basis set can be seen on plots of the flawed isosurfaces for extremely small density values. On the other hand, too high density guess yields a surface which is unrealistically close to the model atoms. In this regime the used approximation is no longer valid anyway.

In all cases the programs, that perform DFT calculations, were set to integrate local density of states within a prescribed energy window. The resulting volumetric data was processed by a separate tool.

1.8 The software packages used

The multitude of existing DFT software packages is overwhelming. Three of them were used to deliver results presented in this work.

The main differences among them are

- choice of the basis set

- form of the pseudopotentials (or alternative method)

- specific optimizations e.g. to leverage sparsity of certain matrices

- algorithms employed to solve eigenvalue problems

1.8.1 The SIESTA method

The software package called SIESTA [42, 43], which was the one most used in this study, was created with systems of thousands of atoms in mind. Care was taken to make computational cost scaling linearly with system size. However, all results from SIESTA presented in this work are obtained with direct matrix diagonalization instead of the special order-N functional.

The basis set employed by this method consists of atomic orbitals of finite size. Arbitrary numerical radial function is multiplied by a spherical harmonic. Their sizes, the cutoff radii can be arbitrary and one can test convergence of the results as they are increased.

There can be multiple orbitals defined per one angular momentum. Typically, two of them (a set called double-ζ) with polarization orbital (DZP) basis is used.

In order to achieve strictly linear scaling in all stages of computation, several new ideas found their implementation in the program. In general, the one-electron states can be found by direct diagonalization, taking cubic time or some sort of optimization, which requires extra effort to keep them orthogonal (usually cubic time too). The authors of SIESTA implemented

an idea that extra terms added to the energy functional will ensure the final states to be orthogonal.

1.8.2 The Quickstep method

Another implementation used in this work, based on the Quickstep [44] method, is contained in the CP2K program. Being carefully designed, it achieves excellent efficiency in parallel environments with thousands of processors.

The method make use of two basis sets: plane waves and atomic orbitals, which are combinations of Gaussians. Wavefunctions can be expanded by the localized atomic orbitals in a space-efficient way. The electronic density is expressed in terms of plane waves.

The program implements the so-called Orbital Transformation method [45]. The Kohn-Sham orbitals are transformed so that the needed constraints are only linear and, at the same time, the procedure is guaranteed to converge.

1.8.3 The VASP package

For best description of electronic states in vacuum regions the the VASP program [46, 47, 48, 49] was employed, because it uses plane wave basis set. The basis can be easily improved by setting a single cutoff value and thus testing convergence of results with respect to the size of the basis is simple.

In practice, with calculations performed for this work, VASP turned out to be computationally more demanding than the other two programs. However, it is useful when an insight into states extending into vacuum is needed, which cannot be well described using orbitals localized on atoms.

Chapter 2

Study of pure InSb and InAs surfaces

2.1   Considered compounds

Indium antimonide is a narrow-gap semiconductor of the III-V family. It found many applications, for example in optoelectronic devices. Many structures are grown by molecular beam epitaxy starting with the surfaces, so it is important to know their exact structure. There are established methods with which clean and flat crystal surfaces can be prepared, ready for measurements and other experimental work.

InSb (and also InAs, the other compound considered in this chaper) crystallizes in a zinc blende structure. The (001) planes coincide with either only indium atoms or only antimony. It was found experimentally that, depend-

ing on the imposed preparation conditions, such (001) surfaces can be made rich in one of the components [50]. During the preparation of a clean crystal surface atoms are exchanged with the gas phase. This process can result in stoichiometry change and influences the final equilibrium geometry of the reconstruction.

It is worthy to note a related research results here. There were observed gallium clusters on one of the Ga-rich GaAs surface reconstructions [51]. They are ordered so that the surface has 4×6 periodicity. The order is not perfect, but it is clearly better than in the case of InSb and InAs discussed here.

2.2 Reconstruction of the InSb(001) surface

Surface of a crystal breaks translational symmetry in one direction. The most obvious consequence of this fact is that the equilibrium positions of atoms change with the distance from the surface. The most distorted structure, in the most asymmetric environment, where atoms struggle to saturate their bonds, is found next to vacuum (or, possibly, interface). The term *surface reconstruction* refers to the structure of these top layers.

Cleaning and annealing of the (001) surface of InSb crystal, performed in an indium-rich environment, usually results in formation of the $c(8 \times 2)$ phase [52]. LEED experiments confirm its presence in broad range of temperatures [2]. The reconstructed surface has high anisotropy and is very reactive, so it

is an interesting template for growing nanostructures.

It is important to note that a disorder was recently observed on this surface by STM in low temperatures [53].

2.2.1 The ζ model

In the past there were proposed models of this surface [54, 55], which contain dimers in the surface layer. They were later found not fully consistent with results of STM measurements.

In the year 2000 a new family of models was proposed independently by two groups. Lee et al [56] found them with *ab-initio* calculations and Kumpf et al [5] derived them from X-ray surface diffraction data for InSb, InAs and GaAs.

The model shown on the Figure 2.1 differs from the above original data, because the atomic positions shown are already optimized by DFT calculations described in Section 2.3. Nevertheless, it retains qualitative similarity to the original model, called ζ.

The most outstanding its feature is presence of subsurface indium dimers. These atoms are labelled In-9 and reside in the first layer below the top bilayer. Other atoms of this layer stay close to their ideal crystal bulk positions. The topmost part of the model, which corresponds to two atomic layers, is heavily reconstructed.

The model features symmetries with respect to the following lines and planes perpendicular to the surface: axes going through In-1 atoms, each
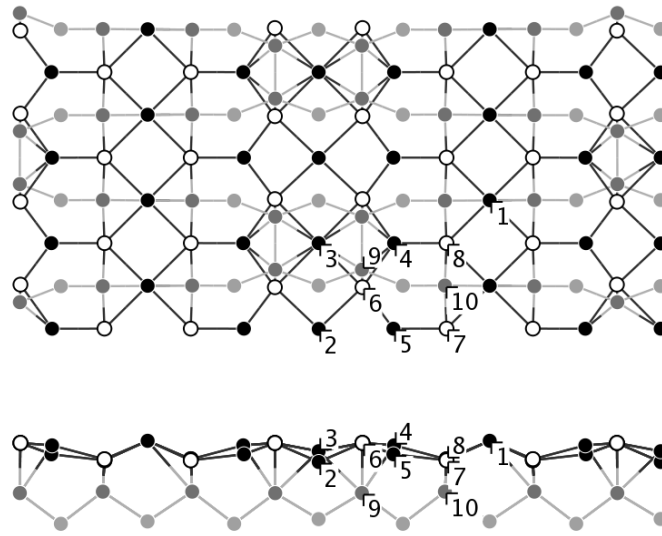
Figure 2.1: DFT-optimized ζ model of reconstruction of the InSb(001) surface with $c(8 \times 2)$ symmetry. Atoms of the top bilayer are shown as black (indium) and white (antimony) discs. The next subsurface layer contains indium atoms (dark grey circles). The atoms labelled In-9 form dimers in this layer. The last displayed surface is a bulk-like layer of antimony (light grey circles).
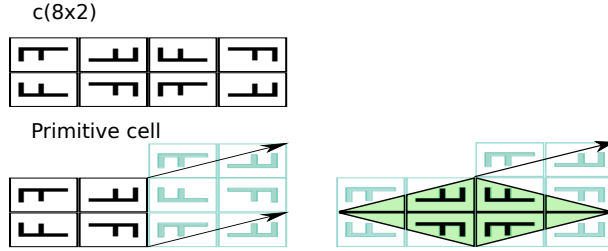
Figure 2.2: A schematic representation of symmetries of the discussed surface reconstruction.

plane situated on In-2,3,4,5 and Sb-7,8 atoms and planes containing positions of In-2 and In-3 (Fig. 2.2). These symmetries are observed by electron diffraction measurements.

A remarkable feature of this structure is that the In-1 atoms, being the most elevated, form outstanding rows in the [110] direction. In-3 are the lowest atoms of the reconstructed bilayer.

The general model found by Kumpf et al describes surface reconstructions of a family of compounds by assignment of different occupation numbers to a selection of sites. In case of InSb, the sites labelled In-1 are about 57% occupied.

2.2.2   The model resulting from this work

This work refines this picture by discovery of mobility of the In-1 atoms. It was also found that they readily form dimers and trimers. The performed calculations show that there are many different low energy configurations in which some of the In atoms are clustered above the row of In-1 sites.

2.3   Theoretical treatment of the surface

Since this is probably the first DFT-level treatment of the InSb(001) $c(8 \times 2)$ surface, the data derived from X-ray experiments [5] was used as a starting point.

Accuracy of a DFT calculation depends on many factors. It cannot be systematically improved by choice of more complex exchange-correlation functional, as there are only several approximations researched in depth. Only some of them are actually implemented in the software packages used in this work. While it would be an interesting undertaking to assess performance of hybrid functionals applied to the systems studied in this work, they are computationally too demanding and thus PBE GGA was used exclusively.

Another parameter affecting calculation accuracy is the basis set size. Set of plane waves used in VASP calculations is defined by a cut-off value, which can be increased for a convergence test. In case of localized atomic orbitals used in Siesta and CP2K, it is harder to increase the basis set and a single setting was used for this work.

In general, in order to accurately treat surfaces, the used localized basis may need to be extended into vacuum [57]. The presented here results obtained with VASP, whose basis uniformly covers all the simulation cell, are free from such concerns. However, more work was done using localized basis, because it allows for lower computational costs. This usage can be justified by comparison of LDOS plots based on Kohn-Sham orbitals delivered by

these two methods. They are shown on Fig. 2.4. Fortunately, the differences are not significant enough to affect how the STM images can be interpreted.

Results obtained for infinitely extended systems depend on fineness of the sampling of Brillouin zone. For all calculations of local density of states, used for STM simulation, it was increased. Number of chosen k-points was limited by available processing power (and also by apparent software failures). In case of structure relaxations with big simulation cells, which correspond to small Brrilouin zones, only the Γ point (zone centre) was engaged.

Apart from the above factors, there are also chosen pseudopotentials, convergence conditions (stopping criteria) and many choices related to particular specific optimizations made to the DFT solvers. These were generally kept at their recommended values found in documentation.

Even if the electronic problem was exactly solved, quality of the problem statement itself remains of importance. The periodic boundary conditions applied in all three dimensions require that care must be taken to represent systems of lower dimensionality. While isolated molecules are adequately approximated by a grid of well separated images and thin films can be simply stacked keeping sufficient vacuum region between them, a half-space occupied by a crystal with a single surface must be cut.

Two decisions must be made about this cut. First, a suitable termination has to be chosen, which would imitate the missing bulk of crystal. For all the surfaces studied here a single layer of hydrogen atoms was chosen as a reasonable way to saturate bonds of the bottom atoms. The added hydrogen
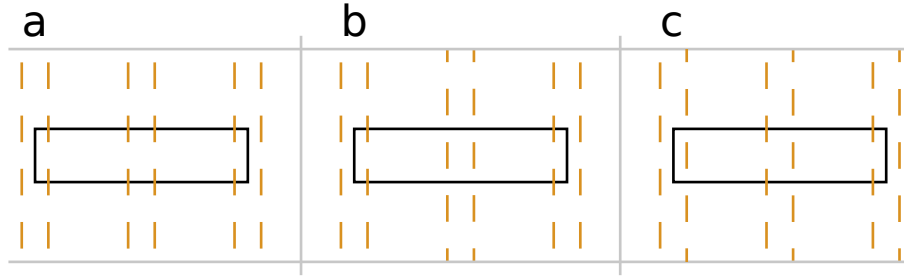
Figure 2.3: Schematic representation of some possible arrangements of In-9 dimers. The rectangles indicate areas of 8×2 size.

atoms are placed at equilibrium distance, but at the would-be lines of bonds to the next missing layer.

Second choice determines the thickness of the retained portion of the crystal. For a given quantity of interest its convergence with respect to increasing the thickness can be checked. This way one can estimate how accurate is, for example, the surface energy obtained with the affordable model sizes. This issue becomes problematic, when derivation of the observed object is costly, as in the case of LDOS plots.

In order to study the discussed reconstruction, several InSb(001) surface models of different thickness were built. Let the symbol Ln mean here a (001) surface model with n bulk-like layers.

Although the available experimental data indicated that about 2/5 of the In-1 sites are vacant, the first examined models were built with all the In-1 positions occupied (four In-1 atoms in the 8×2 unit cell).

Arrangement of In-9 dimers determines structure of the top bilayer and symmetry of the reconstruction. Fig. 2.3b shows it for the $c(8 \times 2)$ model. A

Atom	4 × 2						c(8 × 2)					
	SIESTA			VASP			SIESTA			Experiment [5]		
In-1	2.000	0.506	-0.052	2.000	0.508	-0.051	2.000	0.500	-0.051	2.000	0.500	-0.051
In-2	0.000	1.000	-0.132	0.000	1.000	-0.127	0.000	1.000	-0.270	0.000	1.000	-0.295
In-3	0.000	0.000	-0.223	0.000	0.000	-0.206	0.000	0.000	-0.172	0.000	0.000	-0.203
In-4	0.876	0.000	-0.160	0.880	0.000	-0.146	0.889	0.000	-0.113	0.881	0.000	-0.159
In-5	0.885	1.000	-0.087	0.881	1.000	-0.085	0.887	1.000	-0.154	0.884	1.000	-0.162
Sb-6	0.514	0.483	-0.069	0.509	0.483	-0.063	0.528	0.509	-0.081	0.532	0.511	-0.106
Sb-7	1.496	0.000	-0.209	1.500	0.001	-0.196	1.493	-0.000	-0.200	1.485	0.000	-0.220
Sb-8	1.498	1.000	-0.202	1.499	1.000	-0.190	1.496	1.000	-0.205	1.493	1.000	-0.255
In-9	0.504	0.691	-0.478	0.504	0.690	-0.473	0.511	0.315	-0.502	0.516	0.315	-0.536
In-10	1.476	0.504	-0.466	1.476	0.503	-0.454	1.484	0.497	-0.469	1.483	0.500	-0.490

Table 2.1: Atomic coordinates x, y, z (in LEED units) of the main atoms in the upper layers of the surface shown for two L4 reconstruction models for comparison with the available experimental data [5]. The x and y axes are along the directions $[1\bar{1}0]$ and $[110]$, respectively.

structure of 4×2 symmetry (Fig. 2.3a) was created, also based on the data of Kumpf et al [5]. Note that these two are not all of the possible arrangements (Fig. 2.3c).

For the smaller unit cell of 4×2 size optimal atomic coordinates were calculated with both VASP and Siesta (Table 2.1). Similarity of these results confirm that correct settings and pseudopotentials were used in the calculations.

The Table 2.1 also contains coordinates of the relaxed $c(8 \times 2)$ model which can be compared to the experimental data given in the last column.

The model surface does not undergo significant changes when every second In-1 atom is removed. The simulated STM images (Fig. 2.7) are also similar to the corresponding plots obtained with 100% In-1 occupancy (Figs. 2.6 and 2.5). These results were obtained with Siesta.
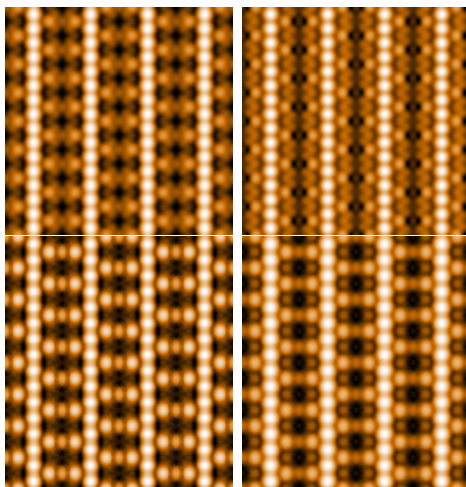
Figure 2.4: Simulated STM images for -1 V (left) and +1 V (right) obtained for the L4 model. Upper and lower plots made with data from VASP and Siesta, respectively.

The CP2K package allows to do DFT calculations with much bigger cells. An InSb surface cell of 8×8 size was created. Energies of pairs of vacancies at different separations were compared. Relaxations of these models resulted in very small corrections of atomic positions. It was found that differences between their total energies are of order of $10^{-2} eV$. It can be therefore safely assumed that there is no preferred distribution of vacancies on this surface (within the set of models considered here).

2.3.1 Simulated STM images

Initially, the models up to L4 were relaxed and convergence of atomic positions of L4 was considered satisfactory. Subsequently, L4 was used as a substrate for the PTCDA adsorption studies described in Chapter 3. Also, a
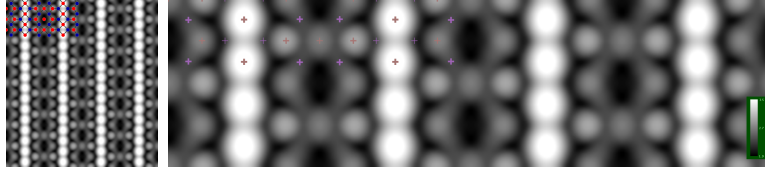
Figure 2.5: LDOS plot for +1 V bias (unoccupied states). Pure InSb(001) surface relaxed in a model with 10 bulk-like layers. All In-1 sites occupied. LDOS calculated in a model with two layers less. Left: overview of an area of 16×16 size. Right: four reconstruction unit cells (total size is 16×4); crosses indicate positions of atoms of the top bilayer.
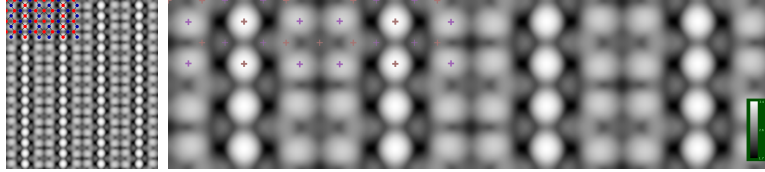
Figure 2.6: LDOS plot for -1 V bias (occupied states). Otherwise identical to the Fig. 2.5.

series of LDOS plots were made with this model. Examples with ± 1 V bias voltages are shown on Fig. 2.4.

It was much later discovered that these results can be improved, because of very minute corrections of atoms positions obtained with L10 model. It is somewhat surprising that a crucial change occurs when the model is extended to be as large as L10. Sb-6 atoms moved up and are visible as bright features (Fig. 2.6), which are no longer dominated by image of In-4,5 atoms (compare to Fig. 2.4, upper left part).

The plots shown on Figs. 2.5 and 2.6 are obtained with the relaxed L10 model cut to L8 size, with the terminating hydrogen layer attached anew. The resulting smaller number of atoms helps to perform computations with
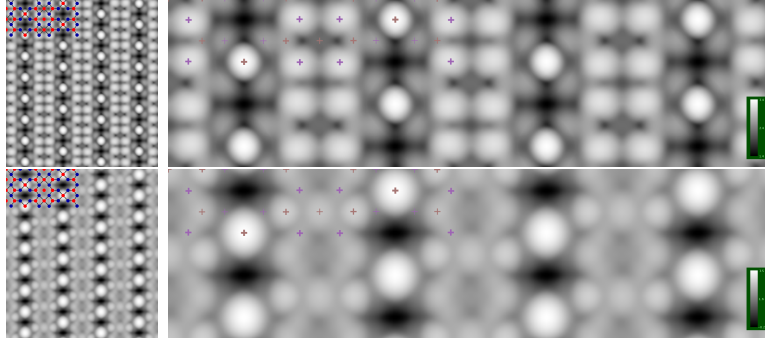
Figure 2.7: Simulated STM imates for -1 V (upper) and +1 V bias (lower plots). 50% occupancy of In-1 sites, otherwise identical structure to the one used for Figs. 2.5 and 2.6.

high number of k-points. The used grid of k-points was generated by 3 divisions along the 8 LEED units long side of the reconstruction cell, and 11 divisions along the short side. There is no point in sampling the Brillouin zone in the direction perpendicular to the surface, as the vacuum region kept between surface images makes the zone flat.

The above presented results pertain to the InSb(001) model with 100% occupancy of the In-1 sites. The model can be made closer to the observed stoichiometry if every second In-1 atom is removed from it. Relaxation of this 50%-occupied model revealed that the overall surface structure is insensitive to the presence of In-1 atoms. Since displacements of atoms are very small, the resulting simulated STM images (Figs. 2.7) are similar to the previous ones, apart from the obvious changes to the appearance of the In-1 row.

The LDOS plots for models with 100% and 50% occupancy of the In-1 rows are shown together with results of low temperature STM in the Fig. 2.8.
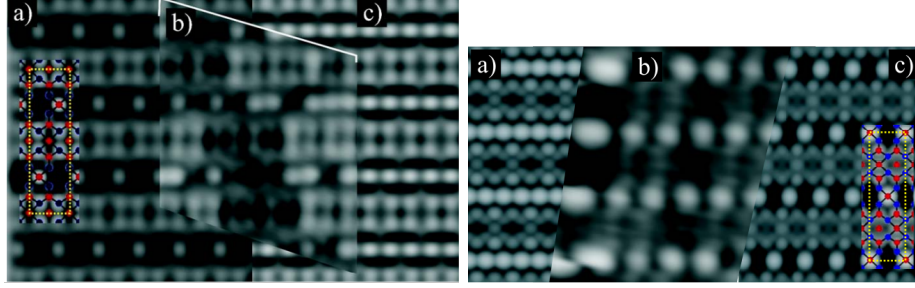
Figure 2.8: Comparison of experimental low-temperature STM images of the InSb(001) $c(8 \times 2)$ surface and the results of calculations presented in this work. The figures are taken from [2]. Bias voltage: -1 V (left), +1 V (right). Both panels contain: a simulated image for 50% In-1 occupancy – left (a) and right (c); (b) experimental data; and a simulated pattern for In-1 row occupied in 100% – left (c) and right (a). The dashed rectangle represents unit cell of the surface reconstruction.

In case of negative bias voltage two main features are observed: dominant rows or separate protrusions representing In-1 atoms and groups of four spots located above the Sb-6 atoms. They are seen the same both in experiment and theory. The microscopic image contains areas of different concentration of In-1 atoms, because the occupancy is between 50% and 100%.

Appearance of the In-1 row in the images of unoccupied states (positive bias voltage) is also consistent. Since lack of contrast between the rows in the STM image is likely caused by worse imaging conditions, the comparison can be considered entirely satisfactory.

2.3.2 Mobility of the In-1 atoms

While the work presented in this thesis progressed, our understanding of both the In(001) $c(8 \times 2)$ surface reconstruction and behaviour of PTCDA

51
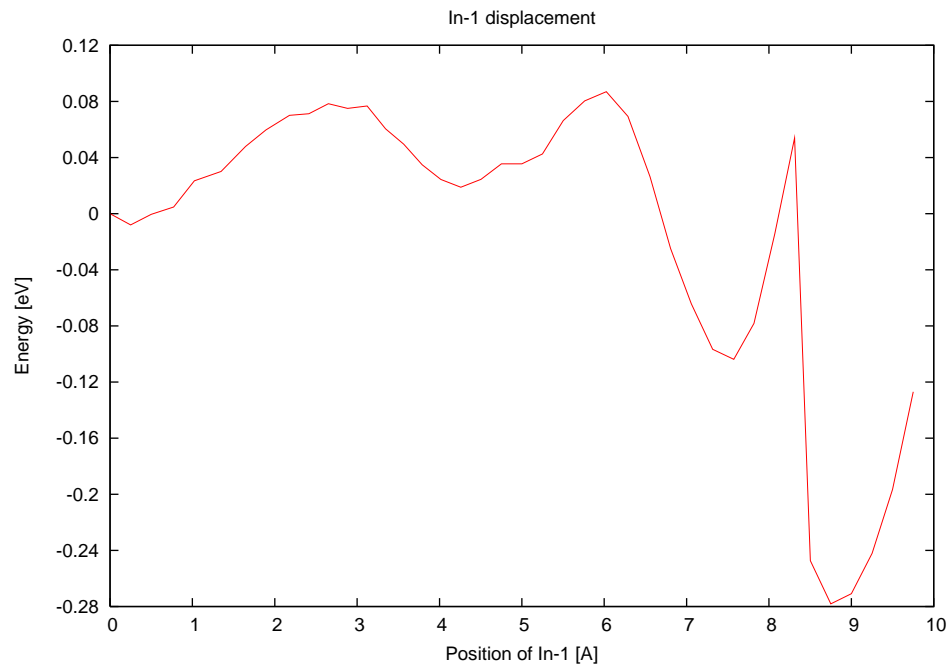
Figure 2.9: Energy of the surface with pushed In-1 atom shown as it changes along its simulated diffusion path along the [110] direction.

molecules adsorbed on it evolved in parallel. The study of diffusion of PTCDA molecule described below in section 3.7 revealed that indium atoms belonging to the In-1 row can be pulled by the adsorbate. Consequently it was supposed that indium atoms encounter little barrier moving along the path formed by pair of rows of Sb-7 and Sb-8 atoms.

In order to verify this hypothesis, a search for a transition path was set up in the manner described in section 1.4.1. Diffusion of a single indium atom was considered. It was pushed along the In-1 row. Steady movement of its projection onto the [110] direction was the only enforced feature of the trajectory to be found. During each optimization step the indium atom of interest was allowed to freely move within a plane perpendicular to the direction of surface rows. The plane was fixed at successive positions pushing the constrained atom for up to 9.75 Å in steps of 0.25 Å (as measured along [110]). All other atoms except the lowest layers of the slab could freely relax in these calculations.

The initial structure used for this simulation (Fig. 2.10) features the In-1 atom to be pushed, which is placed between two vacant In-1 sites. Since all calculations are performed with periodic boundary conditions, the cell needed in this case has to be at least of 8×4 size (in standard LEED units). Such model would have two In-1 rows with four distinct In-1 sites in each. It turned out that among the DFT codes used for this work, CP2K was the fastest for the purpose of this calculation. Its calculations involve only the Γ point of Brillouin zone, hence a large cell of 8×8 size was used. The
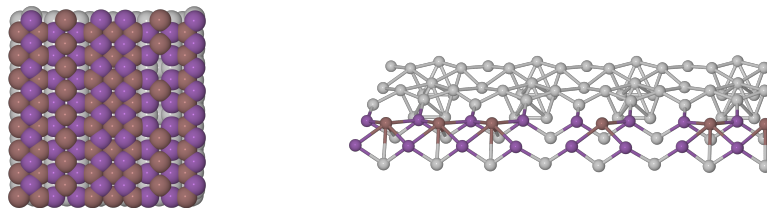
Figure 2.10: The initial structure used for simulation of diffusion of In-1 atoms (top view and side view). The pushed atom is located between the two visible vacancies.

slab consisted of top bilayer and only four bulk-like layers with hydrogen termination, still it contained about 500 atoms in total.

The energy plot (Fig. 2.9) shows barriers it overcomes as the simulation proceeds. The first small barrier of 0.08 eV has its peak where the atom sits just in between Sb-7 and Sb-8 atoms (Fig. 2.11a). The next energy minimum is close to the usual In-1 site, but not precisely at it (Fig. 2.11b). Asymmetry of arrangement of the surrounding atoms causes this slight deviation. The next encountered barrier is similar (Fig. 2.11c). It is followed by sharp decrease in energy caused by formation of an indium dimer (Fig. 2.11d). This structural change yields 0.1 eV relative to the model of Kumpf. The basin of energy surface explored up to now becomes more and more shallow at the constraint plane and disappears when the plane is moved after the 34-th step of the search procedure. The next run of the optimization finds another energy minimum, causing a sudden energy drop. It means that the peak seen at about 8 Å (Fig. 2.9) is higher than the real energy barrier corresponding to the transition. The energy minimum corresponds to a trimer-like structure
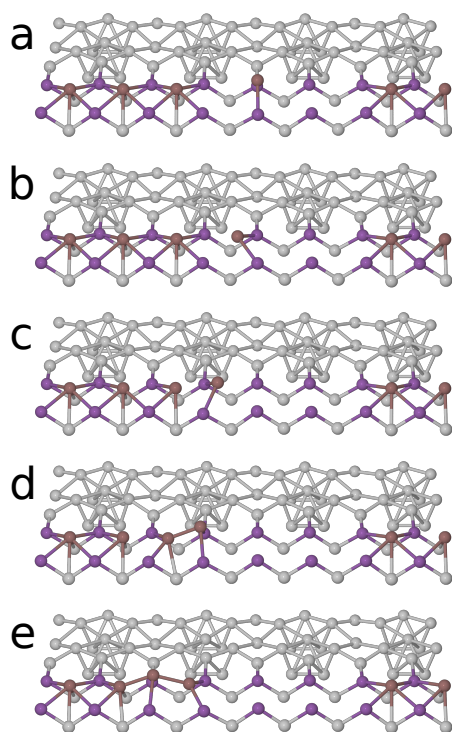
Figure 2.11: Steps of the simulation of diffusion of In-1 atom that correspond to the discussed changes of total energy.
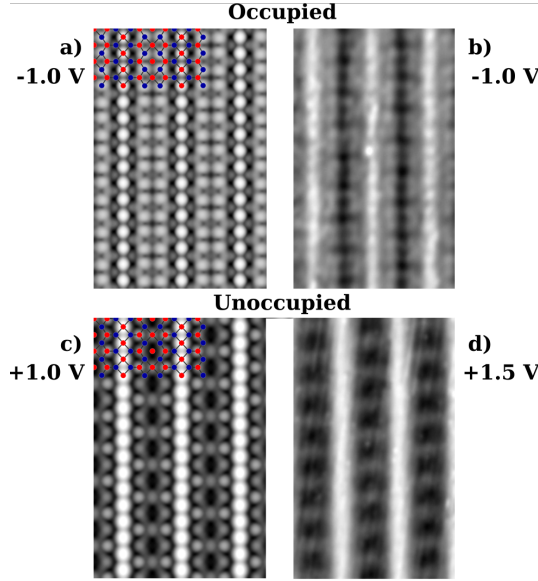
Figure 2.12: Comparison of calculated (left) and experimental STM images taken at room temperature (right). The bias voltages are as indicated. The superimposed surface model contains top bilayer indium (red) and antimony (blue) atoms. Taken from [3].

depicted in Fig. 2.11e.

In light of these results we can state that indium atoms can freely move along the In-1 rows at room temperature. This explains the uniform appearance of these rows observed by SPM. The indium atoms can jump many times while the scanning tip moves from one In-1 site to the next one. Fig. 2.12 shows a room temperature STM scan demonstrating such smearing of the In-1 row. If scans are acquired in low temperature, specific instabilities of In-1 atoms are revealed. Namely, jumps of groups of atoms are witnessed when consecutive lines are scanned over the twin InAs(001) surface [58].

Interestingly, in 77 K, both cluster and chain forms are observed simulta-

neously. This precludes large energy difference between these configurations.

The last, most favourable configuration, the indium trimer deserves more attention. The elevated atom in the bridging position gives rise to an outstanding spot on STM scans, hence it is very good explanation of the brightest features of the STM images acquired in low temperatures. As will be shown in the following section, it turns out that there are other possible arrangements of In atoms close to the In-1 sites, which have similar energies.

2.4 Search for possible structures of indium clusters

Pure theoretical prediction of the structure of the In-1 rows would require comparison of free energies of exhaustive set of arrangements of atoms. This would be most practically conducted in two steps: search for local energy minima and evaluation of curvature of the energy surface in neighbourhood of these points. However, in case of clustering of indium atoms, only the low temperature behaviour can be discovered by SPM experiments. Hence, it is satisfactory to obtain theoretical results near 0 K and assume that entropic effects are negligible.

As said before, simulation of behaviour of PTCDA adsorbed on the surface has led to the discovery of cluster structures of In-1 atoms. The first study of such structure was based on an optimized geometry of PTCDA with additional In atom lifted (Fig. 3.14). The molecule was erased from the
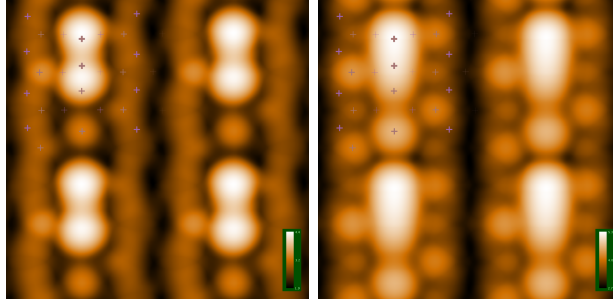
Figure 2.13: Simulated STM image of the first model of cluster structure on the In-1 row. Occupied states with -1 V bias (left) and unoccupied states with +1 V bias (right).

dataset and it was relaxed again. The model is an L4 slab of 4×4 size with four In-1 atoms (100% occupancy).

Surprisingly, the atoms remained roughly at the same positions and the energy turned out to be lower than of the original model slab of the same size with all In-1 atoms in their ideal positions. For this configuration LDOS plots were prepared. Two of them are shown on Fig. 2.13. The structure can be described as an asymmetric indium trimer. Two of the In atoms are substantially elevated, so they could be seen as bright elongated feature on STM images. This is confirmed by the computed plots (Fig. 2.13).

More studies of this phenomenon were conducted with indium arsenide, whose (001) surface exhibits very similar reconstruction if prepared in arsenic-deficient conditions. It is denoted $c(8 \times 2)/4 \times 2$. It means that there are domains of two kinds found in this surface. One is characterized by the $c(8 \times 2)$ symmetry shown on Fig. 2.2. The other differs mainly by location of the In-9 dimers leading to the 4×2 symmetry. Location of the In-9 dimers

determines structure of the top bilayer above. The areas of 4×2 reconstruction can be considered as boundaries of the domains of the 8×2 structure. In case of the discussed indium antimonide surface the 8×2 areas are so large, that the 4×2 reconstruction is rarely observed [58].

The model slab of InAs(001) surface was prepared starting from the coordinates given by Kumpf et al [5]. They were scaled to match the InAs bulk lattice constant optimal for the Siesta settings used.

This way the locally optimal ζ structure with all the In-1 atoms present was obtained. Subsequently, all the In-1 atoms were removed. In place of this row many indium structures were built and examined, as described below.

The primitive unit cell of the 4×2 reconstruction encompasses two In-1 sites that belong to the same row. In order to study clustered arrangements of up to four indium atoms a larger cell of 4×4 was used.

Truly exhaustive search for globally optimal positions of a set of atoms with DFT level of accuracy requires minimal distance between local minima to be assumed. Then the search space can be divided so that all nonequivalent configurations can be enumerated. Number of instances generated this way grows exponentially with the number of atoms. Hence this approach is feasible only in case of the smallest systems.

Fortunately, for the particular system considered here, it is possible to definitely answer the question of the best arrangement of indium atoms over the In-1 row as predicted by DFT.

In order to examine all interesting cases, it is enough to consider eight

sites. In each of them there can be an indium atom or it can be left unoccupied. These are: four In-1 sites of the ideal ζ reconstruction and further four bridge positions (above the point in the middle between two In-1 sites).

These 2^8 cases are enough to solve the problem of low temperature structures forming on the In-1 rows, for the following reasons:

- it is unlikely that a stable structure would consist of three indium atoms stacked vertically

- as experiment shows, there are no elementary structures longer than 4 LEED units forming on the row

- the chosen sites are distant by 0.5 LEED unit and further refinement of spatial resolution would not introduce any new local energy minimum

Some of the configurations were considered unreasonable and excluded from the set. Moreover, the used 4×4 surface slab has translational symmetry, as it consists of two identical halves. Also there is a plane of symmetry going through each As-7/8 pair. An extracted set of inequivalent arrangements contains models with up to 8 indium atoms added.

The most relevant cases among them, which can be compared to experimental results, have 2, 3 or 4 indium atoms in the model cell. This corresponds to 50%, 75% or 100% occupation of In-1 sites.

All the generated models were relaxed. Some of the structures converged to the same stable final geometry. For the most of the optimal structures

LDOS isosurfaces were plotted to serve as approximation of STM images with -1 V (not shown) and +1 V (shown in table 2.2) bias voltages.

In the table 2.2 the results are presented in groups of the same number of indium atoms placed on the surface. The ground state energies are shown relative to the simplest case, in which indium atoms sit close to the positions given by the ζ model. To compare two structures with different number of In atoms it would be necessary to assume particular value of chemical potential. This would not make sense for interpretation of the experiments aimed at the problem discussed here.

The brightest features seen on the plots correspond to the atoms placed on the In-1 row (horizontal line in the middle). There are also In-4/5 rows visible as series of alternating dim and bright spots. As-6 atoms are less exposed on these images.

As we can see, in some cases a high energy gain of 0.56 eV relative to the simple structure (denoted E_4) is achieved. However this is accompanied by significant displacement of In-5/6 atoms, which is not observed experimentally.

Interestingly, the middle of the rectangle given by As-7/8 atoms is not a stable position for indium atoms. Instead, they prefer to stay shifted by 0.21 LEED unit off this position in either direction.

The first case in the table (x3) features a pair of In atoms and a pair of consecutive vacancies. The second case (x5) has every second In-1 site vacant. These geometries have the same energies.

Among structures with 100% In-1 occupancy, the aggregated ones have the lowest energies. The pure ζ structure is by about 0.4 eV less favourable.

Theoretical description of the areas of the surface with $c(8 \times 2)$ symmetry appears to be very similar. A model slab of 8×4 size was used. First calculations have shown that the added In-1 atoms undergo only minor shifts relative to the results previously obtained with the 4×2 model. These shifts adapt atomic positions to the symmetries of the 8×4 model, otherwise the structure remains the same. Hence, it can be expected that all the solutions for 4×2 lattice apply to the $c(8 \times 2)$ case as well.

One remarkable property of the InAs surface studied here is that the equilibrium positions of the indium atoms that belong to the In-1 rows are not at the exact In-1 sites dictated by the ζ model. They prefer to move along [110] towards the point between As-7 and As-8, thereby breaking the symmetry. This observation explains certain features seen in the experimental STM images [58].

In-1	Initial	Label	Relaxed	LDOS	Energy
0.5	o●o●o o	x3			$E_{x3} = 0.00\text{eV} + E_2$
0.5	o●o o●o	x5			$E_{x5} = E_2$
0.5	o o●o●o	x6			$E_{x6} = -0.05\text{eV} + E_2$
0.5	o o●o o●	x10			$E_{x10} = -0.00\text{eV} + E_2$
0.5	o 8 8 o	x48			$E_{x48} = -0.29\text{eV} + E_2$
0.75	o●o●o●o	x7			$E_{x7} = E_3$
0.75	o●o8●o o	x19			$E_{x19} = -0.04\text{eV} + E_3$
0.75	o o●8●o	x38			$E_{x38} = -0.17\text{eV} + E_3$
1.	o●o●o●o●	x15			$E_{x15} = E_4$
1.	o●8 o●o●	x29			$E_{x29} = -0.56\text{eV} + E_4$
1.	o●8 8●o	x53			$E_{x53} = -0.44\text{eV} + E_4$
1.	o 8●8 o●	x58			$E_{x58} = -0.56\text{eV} + E_4$
1.	o●8●o 8	x83			$E_{x83} = -0.23\text{eV} + E_4$
1.	o●8 o●8	x85			$E_{x85} = -0.40\text{eV} + E_4$
1.	o 8●o●8	x86		(no image)	$E_{x86} = -0.64\text{eV} + E_4$
1.	o o●8 o●●	x170		(no image)	$E_{x170} = -0.54\text{eV} + E_4$

Table 2.2: Results of the search for low-energy configurations of the indium atoms in the In-1 surface row. Columns contain: occupancy of the In-1 sites, initial structure – a side view with indium atoms (dark circles) and As-7,8 atoms (white discs), a label, side view of the relaxed structure, simulated STM image for unoccupied states, energy shown relative to the ideal models which contain n indium atoms occupying the In-1 sites. They are based on ζ and their energies are denoted E_n.

Chapter 3

Adsorption of PTCDA molecules

Perylene-3,4,9,10-tetracarboxylic dianhydride (PTCDA, Fig. 3.1) is widely studied as a model organic semiconductor [59]. In particular, its adsorption on a variety of surfaces was examined and structures of the thin layers it forms were determined.

The molecule is planar with a core consisting of aromatic rings. The calculations presented here show that it bends significantly when deposited on the InSb(001) surface. This enables formation of chemical bonds. Mobility of the molecule is essentially constrained to one dimension.
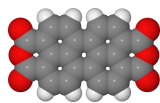
Figure 3.1: Model of the perylene-3,4,9,10-tetracarboxylic dianhydride (PTCDA) molecule consisting of oxygen (red spheres), hydrogen (white) and carbon (grey) atoms.

The most important and most readily available outcome of theoretical modelling of the molecule adsorption are: positions of atoms in the energetically most favourable configurations, deformations of the involved parts, accompanying change of distribution of electrons and several energy differences, which are explained in detail in the following section.

One could also examine shape of energy wells of the energy surface (as discussed in Section 1.2), especially the relevant energy barriers. This would lead to finite temperature considerations, i.e. comparison of free energies of the considered adsorption geometries, but it is beyond the scope of this work.

3.1 Description of the adsorption in terms of energy

Consider two parts of an atomic system, called A and B. In particular, let A_0 and B_0 denote their configuration unperturbed by external interactions (vacuum state) of the lowest energy. They can form a combined system, denoted AB when they come close together, in our case driven by simple adsorption process. In a response to a new neighbourhood the atoms change their positions and the resulting deformed geometries, being different than A_0 and B_0, will be denoted here as A and B.

It is crucial to compare energies of the two considered states of the two parts: staying far apart and interacting in the combined system. Thus we

define an adsorption energy, in the following way:

$$E_{ads} = E_{A_0} + E_{B_0} - E_{AB}$$

Positive value of E_{ads} indicates that formation of the combined system is preferred, provided that its temperature is low enough. This extra assumption stems from the fact, that entropic effects are entirely neglected here since we study only isolated points in phase space.

The energy expenditure for shape change of the constituents is called deformation energy:

$$E_{def} = E_{def}^A + E_{def}^B = E_A - E_{A_0} + E_B - E_{B_0}$$

We can say that the energy gain originating from interaction between the parts, has to make up for the deformation and what remains is the E_{ads} mentioned above. Therefore we define interaction energy E_{int}, which satisfies:

$$E_{int} - E_{def} = E_{ads}$$

All the above energies can be determined by DFT calculations with relaxation of atomic positions. This direct scheme is simple, but better precision can be achieved incurring little additional cost, by looking more carefully at the inaccuracies which appear here.

In DFT calculations, the used basis set is finite and thus incomplete. It

is chosen as small as possible for the required accuracy to save processing power. The error introduced in this way can be reduced by extrapolation procedures and also by simple subtraction of energies of systems that are similar enough. We can usually expect that the error is largely cancelled in the energy difference, because basis set truncation overestimates the energy in the two systems in a very similar way.

If the basis set depends on positions of atoms, as in the case of atom-centred orbitals, we can no longer benefit from the above cancellation as the error introduced by basis set truncation can be different for a two systems, which we want to compare. In practice it is the case, if the DFT method we use is not based on plane waves.

This is especially important for determination of adsorption energies. We compare the energies $E_{A_0} + E_{B_0}$ and E_{AB}. As the combined system AB is formed, some atoms get new neighbours, and so more basis orbitals become available for the electrons. This can reduce the basis set truncation error significantly.

In order to regain the accuracy of E_{ads}, extra intermediate geometries A and B, the deformed but non-interacting parts are considered. It is then possible to calculate energies of the parts with the larger basis corresponding to AB. This leads to the so-called counterpoise formula [60, 61].

Let E_i^j denote energy of system i as calculated using the basis set prepared for the geometry j. E_i^∞ are fully converged energies which could be obtained with a high quality basis.

Energy differences $E_i^{j \to k}$ are defined so that:

$$E_i^j = E_i^{j \to k} + E_i^k$$

We aim at cancellation of errors related with the basis AB. Therefore we rewrite the energies $E_{A_0}^\infty$ and $E_{B_0}^\infty$ in the following manner, keeping in mind that A and A_0 are similar:

$$E_{A_0}^\infty = E_{A_0}^{\infty \to A_0} + E_{A_0}^{A_0} \approx E_A^{\infty \to A} + E_{A_0}^{A_0} = E_A^{\infty \to AB} + E_A^{AB \to A} + E_{A_0}^{A_0}$$

The adsorption energy becomes:

$$E_{ads} = E_{A_0}^\infty + E_{B_0}^\infty - E_{AB}^\infty \approx$$

$$\approx E_A^{\infty \to AB} + E_A^{AB \to A} + E_{A_0}^{A_0} + E_B^{\infty \to AB} + E_B^{AB \to B} + E_{B_0}^{B_0} - \left(E_{AB}^{\infty \to AB} + E_{AB}^{AB} \right) =$$

$$= \left(E_A^{\infty \to AB} + E_B^{\infty \to AB} - E_{AB}^{\infty \to AB} \right) + E_{A_0}^{A_0} + E_{B_0}^{B_0} - E_{AB}^{AB} + \left(E_A^{AB \to A} + E_B^{AB \to B} \right)$$

The first term in parenthesis is small and thus neglected. The last two terms are called basis set superposition error:

$$E_{BSSE} = E_A^{AB \to A} + E_B^{AB \to B}$$

The resulting formula contains explicit correction of the adsorption energy:

$$E_{ads} = E_{A_0}^{A_0} + E_{B_0}^{B_0} - E_{AB}^{AB} + E_{BSSE}$$

In order to determine its value, four extra calculations are required, two with the ordinary basis (E_A^A and E_B^B) and two with the enriched basis set: E_A^{AB}, E_B^{AB}. The added basis orbitals are placed where atoms of the AB system are, but no new electrons nor nuclei are introduced. In case of SIESTA, they are called ghost atoms.

The energies calculated for the PTCDA/InSb system and presented below include the BSSE correction.

3.2   Related research

An example of large organic molecule adsorbed on the InSb(001) surface is given in [62]. The STM results made possible to determine the preferred adsorption sites. Similar to the PTCDA/InSb(001) case, the Violet Lander molecules adjust their geometry to the structure of surface reconstruction. As with PTCDA, molecular chains were observed. However, they form only at the step edges, whereas there is no correlation between conformations chosen at flat terraces. Interpretation of the images with sub-molecular resolution obtained in low temperature requires certain assumptions to be made. Similar uncertainties related to PTCDA appearance were solved by this work.

3.3   First series of relaxations of adsorbed PTCDA

A model surface slab of sufficient size is needed to examine all orientations of the molecule. The 8×2 cell is too small for a PTCDA longer axis oriented along the direction of In-1 rows. Enough room is found in a supercell of 8×4 size, but a L4 model of this size contains 256 atoms. DFT calculations with this model would be too heavy for systematic search for the best adsorption sites.

It was therefore necessary to approximate the $c(8 \times 2)$ reconstruction cell. The top bilayer has almost 4×2 symmetry, lowering of which is primarily caused by the In-9 dimers. Therefore it is reasonable to use half of the cell as its approximation. At this point it is not important how exactly the 8×2 cell is divided (there are basically two possibilities), because the results will be later verified using the full surface model.

Consequently, the model surface slab used at this stage was of 4×4 size and consisted of two 4×2 primitive cells. For simplicity, its In-1 row was fully occupied.

The molecule was placed parallel to the surface in several places. Three orientations were used: $0°$, $90°$ and $45°$ with respect to the In-1 surface rows.

Initially, the relaxations were done in two stages: the L2 model was used first, then two layers were added so it became L4. It was found that no considerable speedup is achieved this way, so most optimizations were subsequently done in one stage.

α_0	x_0	y_0	x_f	y_f	E_{int}	E_{def}^{InSb}	E_{def}^{PTCDA}	β	E_{BSSE}	E_{ads}
0°	0	0	-0.00	-0.00	-3.51	0.43	1.00	34°	0.45	-2.08
45°	0	0	-0.03	-0.01	-3.59	0.41	0.87	31°	0.46	-2.31
90°	0	0	0.00	0.00	-1.76	0.08	0.18	4°	0.36	-1.50
0°	1	0	0.97	-0.00	-3.17	0.61	0.66	22°	0.44	-1.90
45°	1	0	0.97	0.09	-2.94	0.42	0.59	19°	0.40	-1.93
90°	1	0	0.58	0.01	-3.58	0.30	0.63	18°	0.47	-2.65
0°	2	0	2.01	-0.01	-3.65	0.28	1.17	39°	0.46	-2.20
45°	2	0	1.98	-0.01	-2.15	0.20	0.60	21°	0.30	-1.36
90°	2	0	2.01	0.00	-1.01	0.04	0.08	8°	0.26	-0.89
0°	0	1	-0.00	1.00	-3.52	0.43	1.01	34°	0.45	-2.07
45°	0	1	-0.02	0.98	-3.52	0.29	0.84	29°	0.46	-2.39
90°	0	1	-0.00	1.00	-1.76	0.08	0.17	4°	0.36	-1.51
0°	1	1	0.97	1.00	-3.14	0.59	0.65	21°	0.43	-1.90
45°	1	1	0.99	1.08	-2.84	0.36	0.61	21°	0.40	-1.87
90°	1	1	0.59	0.99	-3.59	0.30	0.64	19°	0.47	-2.65
0°	2	1	2.01	1.00	-3.69	0.28	1.19	40°	0.46	-2.22
45°	2	1	2.00	0.99	-1.76	0.24	0.16	11°	0.33	-1.36
90°	2	1	2.00	0.99	-1.03	0.04	0.09	9°	0.26	-0.89
90°	1	0.5	0.47	0.51	-3.83	0.19	0.71	23°	0.47	-2.92

Table 3.1: Results of the first systematic search for the optimal adsorption site of PTCDA in the InSb(001) $c(8 \times 2)$ surface. α_0, x_0 and y_0 is the initial position of the molecule (orientation and two coordinates in LEED units). x_f and y_f are the corresponding final coordinates (in the relaxed system). The β is the bending angle of the molecule explained by Fig. 3.2.
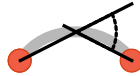
Figure 3.2: Definition of the bending angle β used in the Table 3.1. The three points are averages of positions of the corresponding atoms. The red circles denote the oxygen atoms of the molecule.

The table 3.1 summarizes the results of relaxation of these models. First three columns describe initial positions of the molecule. Here, x names the axis perpendicular to the In-1 rows and the axis y is parallel to it. The initial x and y coordinates shown in second and third column and the final coordinates found in two next columns are given in LEED units, a. Distance between two consecutive In-1 atoms is a. Diagonal of a face of the crystal-lographic unit cell of bulk InSb has length of $2a$. The energies are given in electronvolts and their exact meaing is explained in section 3.1.

The last line of the table is a result of examination of an extra case added when it became apparent that choice of $\alpha_0 = 90°$ and $x_0 = 1$ leads to high adsorption energies.

Final coordinates of the molecule centre are shown in the Table 3.1 as x_f and y_f for the $[1\bar{1}0]$ and $[110]$ (along the In-1 rows) directions respectively. Orientation of the molecule did not change considerably during optimization in all cases. Also, the y coordinate changed only slightly in the process. However, in the cases with $\alpha_0 = 90°$ and $x_0 = 1$, when the molecule placed along the In-4,5 row with its centre above it, it prefers to move by about half of LEED unit towards the In-1 tow to be able to form four O-In chemical bonds.

The first conclusion drawn from these calculations is that the four corner oxygen atoms of the PTCDA molecule readily form bonds with the indium atoms of the surface.

In all calculations the In-4,5 atoms remained immobile. Together with
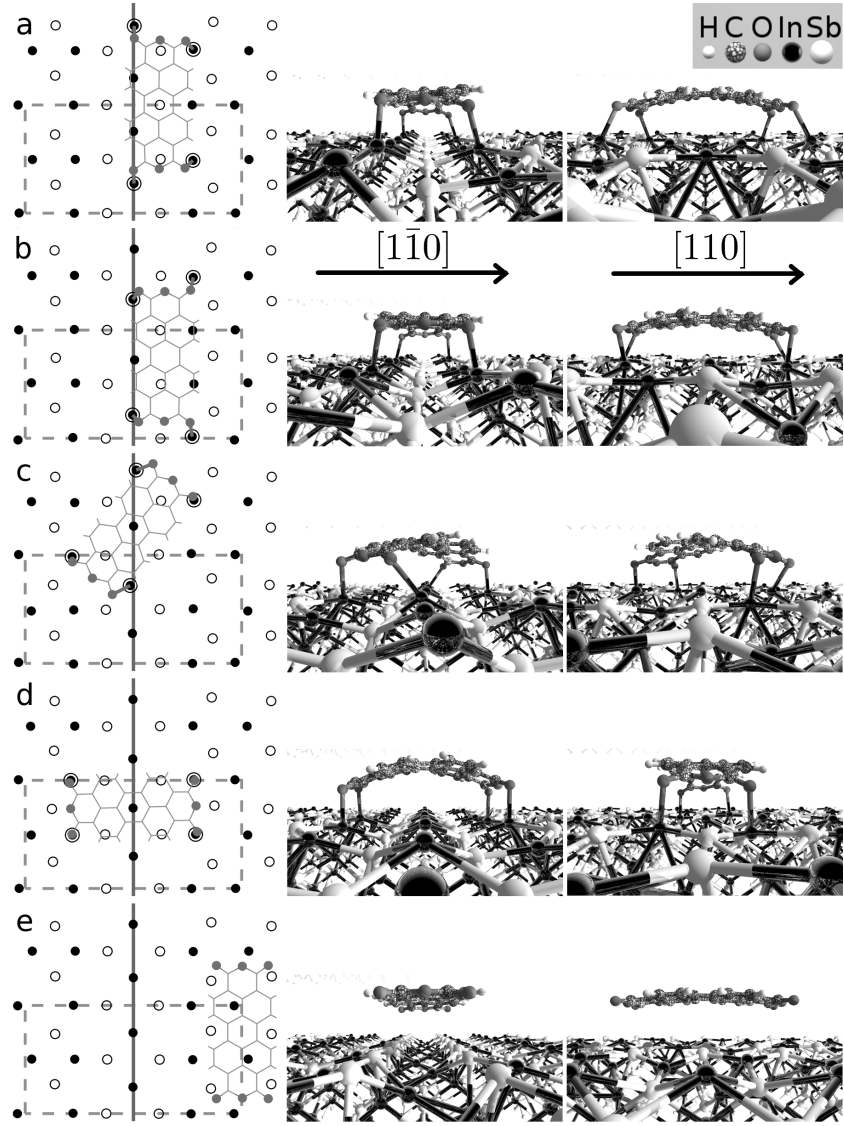
Figure 3.3: Examples of relaxation results. The first column shows a top view of the structures. Indium atoms are marked with black circles, antimony – white circles, oxygen – grey circles. The row of In-1 atoms is indicated by a vertical line. The primitive cell of 4×2 size used in these calculations is shown with a dashed rectangle. The ball-and-stick models show side-views of the same structures. The shown cases are: $\alpha_0 = 90°$, $x_0 = 1$, $y_0 = 0.5$ (a), $\alpha_0 = 90°$, $x_0 = 1$, $y_0 = 0$ (b), $\alpha_0 = 45°$, $x_0 = 0$, $y_0 = 1$ (c), $\alpha_0 = 0°$, $x_0 = 0$, $y_0 = 0$ (d), $\alpha_0 = 90°$, $x_0 = 2$, $y_0 = 0$ (e).

the indium atoms freely moving along the rows of In-1 sites, they are of particular importance for the adsorption of PTCDA. These lines and the In-4,5 sites act on the surface as a pattern that determines possible orientations and positions where the molecule can be anchored.

In order to gain further insight into this interaction, a charge redistribution in the system was calculated as follows. First, the density of electrons in real space was obtained for the full system in its relaxed state, name it $n_{AB}(r)$. Then the density was calculated for each component separately with atomic positions taken exactly from the optimized combined system. These are $n_A(r)$ and $n_B(r)$. The difference

$$\Delta n(r) = n_{AB}(r) - n_A(r) - n_B(r)$$

describes effects of interaction of the two parts. Such redistribution of charge density can indicate chemical binding. Result of the analysis performed for the molecule and the substrate in one of the low energy configurations is depicted on Fig. 3.4. There are clearly visible signs of formation of four bonds between the molecule and surface indium atoms.

Simple examination of the stable atomic positions can also help to identify the binding. For each of the four corner oxygen atoms its nearest neighbouring indium atom was chosen. Distances between these O-In pairs were added. Fig. 3.5 is a plot of interaction energy E_{int} as a function of this sum of distances d. The visible clusters of data points correspond to configurations

74
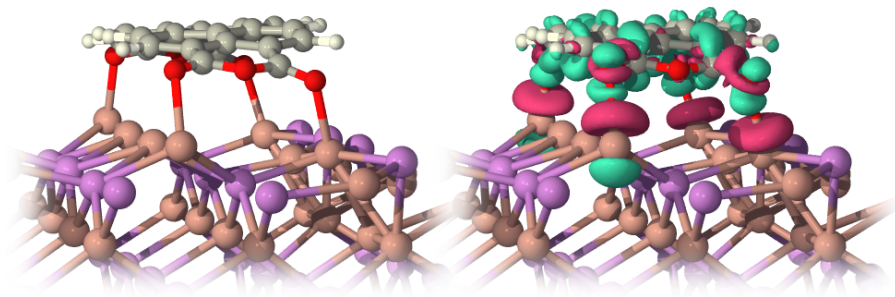
Figure 3.4: Geometry of high binding energy that corresponds to the results shown in the last line of Table 3.1 (left) with a corresponding charge density difference plot (right). Red and green surfaces indicate depletion and excess of electrons, respectively. They are plotted for -0.017 and +0.017 electron/Å^2 density differences.

with different numbers of bonds as counted by simple distance criterion: four bonds for $d < 1.1$ nm, three for $1.1d < 1.35$ nm and less for higher d. Hence, it can be said that each O-In bond brings an energy gain of order of 0.5 eV. The actual bonds have lengths between 0.24 and 0.27 nm.

This extra energy available makes it possible for the molecule to bend substantially.

Because various atomic structures can be found in the In-1 row, it can be expected that there are many stable geometries possible in a real PTCDA/InSb(001) system, all of which share the same basic features: long axis of the molecule oriented along the [110] direction and four corner oxygen atoms bound to In-1, In-4 and In-5 atoms of the surface.

As discussed in Section 2.2.1, the InSb(001) $c(8 \times 2)$ reconstruction cell is symmetric with respect to a plane which contains the In-1 row of the highest atoms. Therefore each existing stable adsorption geometry has a symmetric
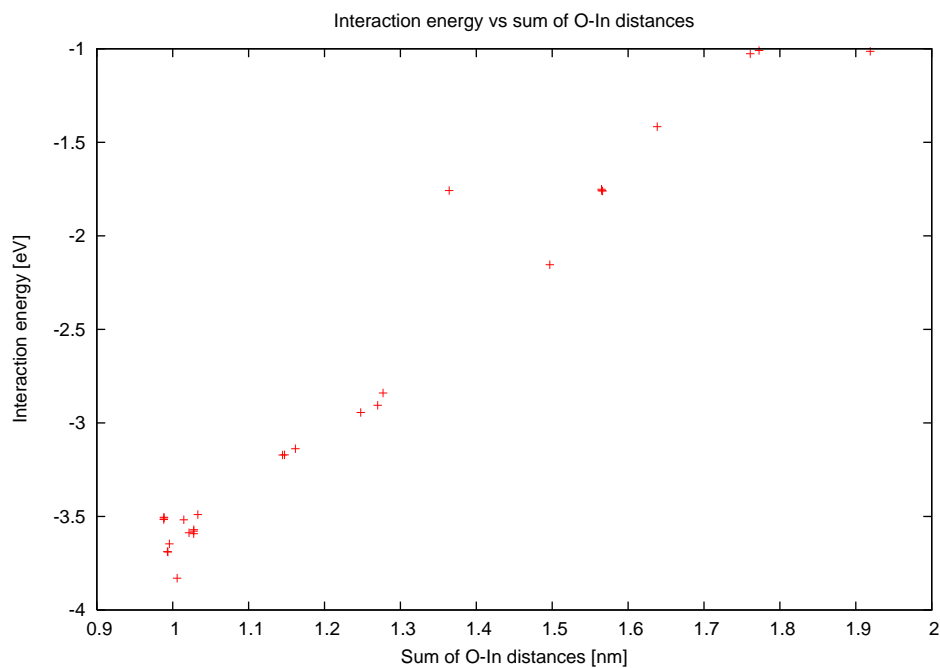
Figure 3.5: Interaction energies E_{int} of all the considered stable PTCDA adsorption sites plotted against sum of four O-In distances. These four pairs of atoms are selected to look at chemical bonds: for each corner oxygen atom of the PTCDA molecule a nearest indium atom was chosen.
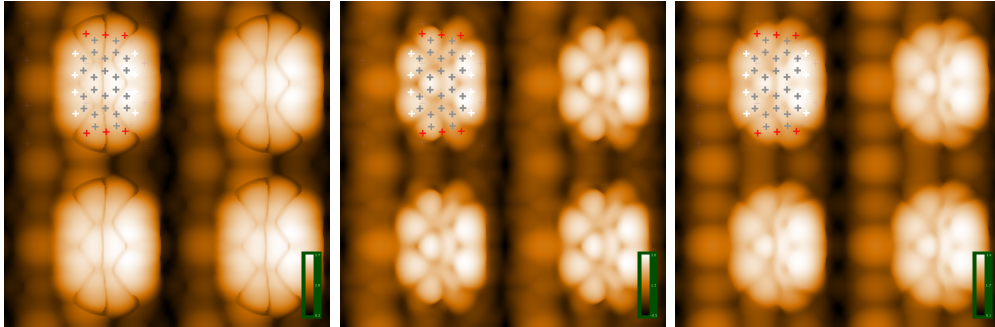
Figure 3.6: LDOS plots for the most favourable adsorption geometry without significant displacements of In-1 atoms (the case with $\alpha_0 = 90°$, $x_0 = 1$, $y_0 = 0.5$). Bias voltages are (left to right): -1 V, -0.05 V and +0.2 V. Crosses indicate exact positions of molecule atoms: hydrogen (white), oxygen (red) and carbon (grey).

counterpart. They should appear with equal probability in experiments.

3.4   Simulated STM images of the adsorbed molecule

In order to allow direct comparison of the above results with experimental findings and to help to interpret it, plots of isosurfaces of local density of states were prepared. As explained in section 1.7, they serve as simulated STM images. Examples for three bias voltages are shown on Fig. 3.6.

All of them are remarkably similar. A dark vertical line in the middle of image of the molecule is a trench in the isosurface that splits it in two halves. The left one, located above the In-1 row, is dimmer. This difference in the appearance of the two halves is caused by a minor tilt of the molecule, a rotation around a line in the [110] direction. It raises four hydrogen atoms so that they give rise to the brightest part of the image.
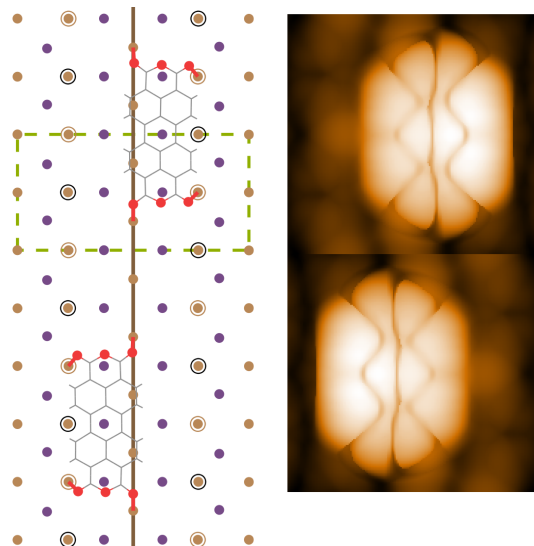
Figure 3.7: Calculated STM images of a low energy configuration ($\alpha_0 = 90°$, $x_0 = 1$, $y_0 = 0.5$) (right panels) shown for two possible positions of the molecule (left panels) with respect to the In-1 row indicated by the solid line ($V_t = $-1.0 V). The In-1 rows in both STM images are aligned with each other for convenience.

The case of low voltage essentially probes the orbitals at the Fermi energy E_F. Very similar results were obtained when the states were integrated on either side of E_F.

The image simulated for -1 V bias voltage shows occupied states. It is similar to the lowest unoccupied molecular orbital of free PTCDA. Indeed, energy levels of the molecule lie relatively low compared to the E_F imposed by the surface, as discussed in section 3.6.

The surface symmetry (see Fig. 2.1) is such that both sides of an In-1 row can equally serve as a adsorption site (Fig. 3.7). This can be most easily observed where two molecules sit close together. Their relative position in-
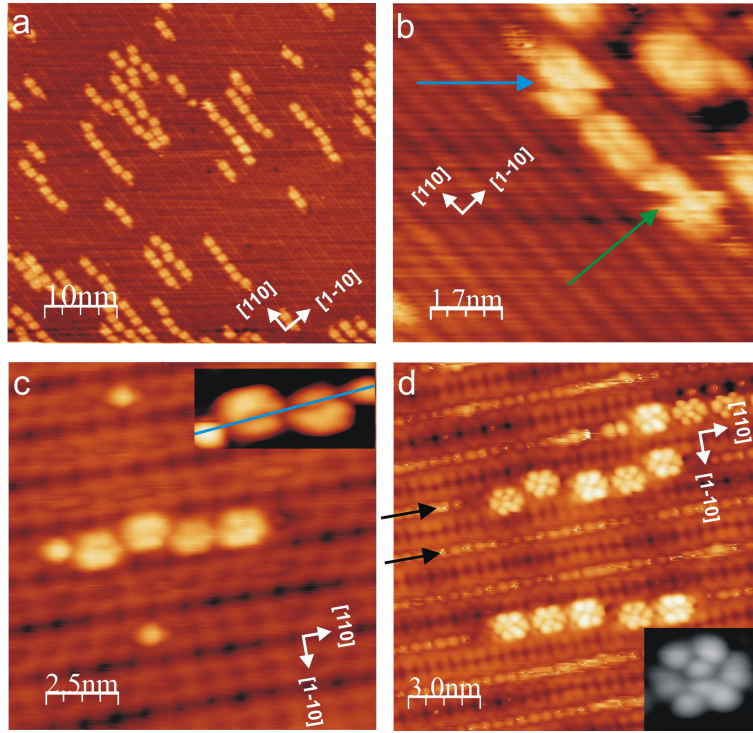
Figure 3.8: STM images of PTCDA molecules adsorbed on the InSb(001). This illustration is taken from [4]. (a), (b) room temperature, $V = -2.0$V; (c) 77 K, $V = -1.0$V; (d) 77 K, $V = 0.5$V. A high resolution image of a single PTCDA molecule is shown in the inset.

cludes a displacement in the $[1\bar{1}0]$ direction, if they choose to occupy opposite sides of the row. The appearance of such pair of PTCDA molecules predicted by DFT calculations can be roughly predicted by simple composition of two simulated STM images. The right panel of Fig. 3.7 consists of two such plots, one of which is a mirror image of the other. This prediction agrees very well with actual observations of the molecular chains (see Fig. 3.8d).

3.5 Relaxation of PTCDA with the full surface model

With basic understanding of the adsorption mechanism, three models of PTCDA put on the full model of InSb(001) $c(8 \times 2)$ surface were built. The system was accommodate to the size of PTCDA by extension of the surface to 8×4 size.

Every second atom of a In-4,5 row, the In-4 atom, is higher by 0.27 Å than In-5. Two atoms of this row are bound to the molecule. There can be two or one atom of this row between them. Hence, the molecule can be bound either to two In-5 atoms or to two In-4 atoms or with In-5 and In-4.

Only three distinct possibilities are possible if the substrate has ideal $c(8 \times 2)$ reconstruction with In-1 sites occupied in 100%. A full model with In-1 mobility and vacancies would likely admit more stable configurations, but all having the same basic properties.

The table 3.2 and the figure 3.9 shows the results obtained with the full $c(8 \times 2)$ surface model. The highest binding energy is achieved in case one chemical bond is formed with In-4 atom and another one is formed with In-5 atoms.

Note that the deformation energy of the surface E_{def}^{InSb} in the first case is negative. There is no indication of mistake, since the ζ structure used here is not the ground state. Hence, an accidental lowering of the energy is not surprising. However, the considered very minute correction of InSb energy
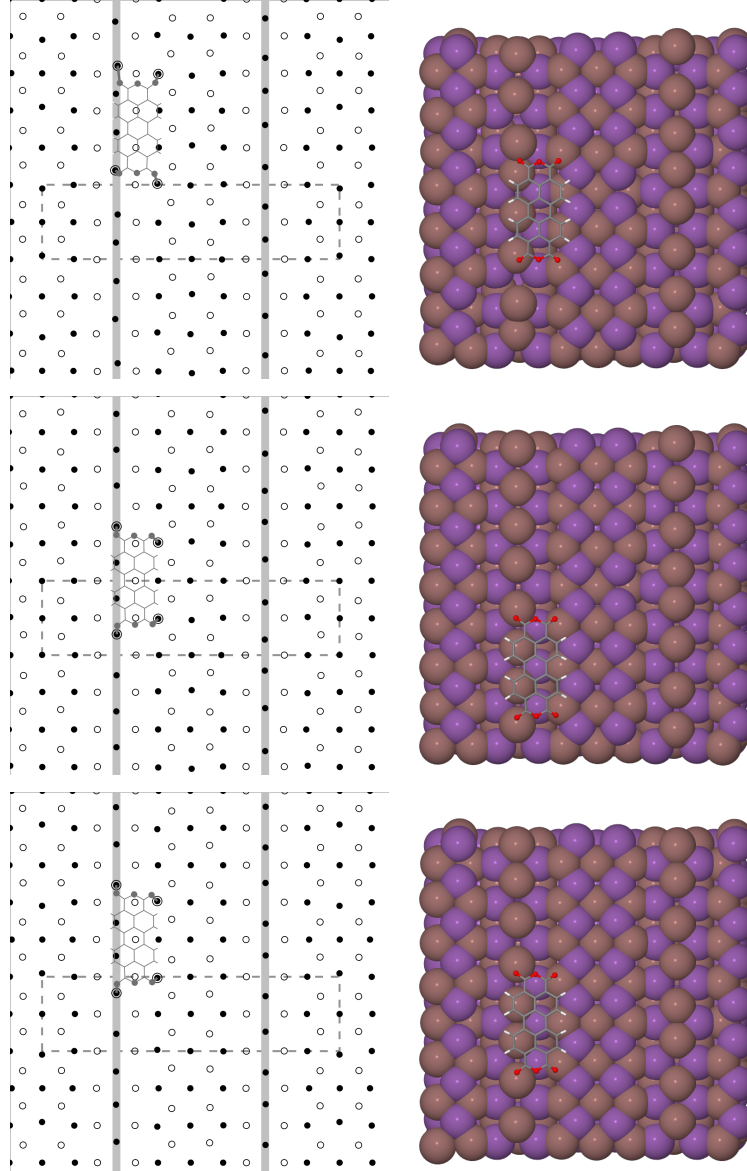
Figure 3.9: The three adsorption sites considered in the calculations with $8{\times}4$ surface cell. The order is the same as in the table 3.2. Gray lines indicate the In-1 rows. The dashed line encompasses 8×2 surface reconstruction cell. Atoms are shown in black (indium), white (antimony) and gray (oxygen).

atoms bound to O	β	E_{int}	E_{def}^{InSb}	E_{def}^{PTCDA}	E_{BSSE}	E_{ads}
In-1, In-1, In-5, In-4	16°	-3.73	-0.02	0.58	0.49	-3.18
In-1, In-1, In-4, In-4	21°	-3.76	0.08	0.66	0.47	-3.01
In-1, In-1, In-5, In-5	24°	-3.85	0.03	0.72	0.47	-3.10

Table 3.2: Results of relaxation of the three structures built on the full $c(8\times2)$ surface model. All energies are reported in eV.

does not correspond to any qualitative change of the model.

3.6 Charge transfer

Isolated molecule in a vacuum features a discrete density of states, which essentially enumerates its orbitals. Interaction of an adsorbed molecule with a substrate mixes them with the surface states so the DOS peaks are smeared [63]. Moreover, in a combined system of surface with a molecule a common Fermi level must be established.

In case of PTCDA adsorbed on the InSb surface, the potential well of the molecule is effectively deeper, so some electron density is transferred to the molecule.

In order to calculate the amount of charge transferred in the considered systems, total charge in real space was obtained with the Siesta program in a form of volumetric data. Two integration volumes were delimited in the simulation cell. It was divided using the following criterion: a given point is included in the first volume if the atom that is closest to it belongs to the molecule. This is essentially a part of a Voronoi diagram.
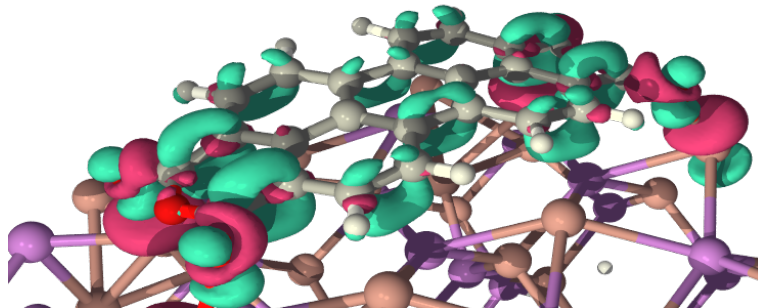
Figure 3.10: Charge redistribution (the same as in Fig. 3.4) showing ten π orbitals filled.

Cases presented in Tabs. 3.2 and 3.1	Transferred charge
In-1, In-1, In-5, In-4	$2.35e$
In-1, In-1, In-4, In-4	$2.12e$
In-1, In-1, In-5, In-5	$2.16e$
$\alpha_0 = 90°$, $x_0 = 1$, $y_0 = 0.5$	$2.03e$
$\alpha_0 = 90°$, $x_0 = 1$, $y_0 = 2$	$2.27e$

Table 3.3: Charge transferred to the molecule in its energetically most favourable configurations. First three entries are results of calculations with the full surface model of $c(8 \times 2)$ symmetry. They are shown in the Table 3.2.

The Table 3.3 shows the resulting charges. They are all above $2e$. The molecule is charged negatively. This is relatively large in comparison to the transfers reported for metallic surfaces [64].

Close examination of the charge difference shown in Fig. 3.10, reveals that some electron density migrates to several of the π orbitals of the perylene core. Similar phenomenon was discovered taking place in the PTCDA/Ag(111) system [65].

This result explains the similarity between LUMO of free PTCDA (shown

in e.g. [65]) and the STM images for occupied states of the adsorbed molecule.

3.7 Diffusion of the molecules

Chains of PTCDA molecules are clearly visible on STM images like Fig. 3.8(a). To help understanding of their formation process, a next problem was stated: how the molecules can move on the surface. For this, two diffusion processes were simulated: one driven along the In-1 rows (the [110] direction) and one across ([1$\bar{1}$0]).

The method of series of constrained optimizations, described in section 1.4.1, was used for this task. In our case, the model, that is, the molecule and a surface slab of 4×4 size, consists of 166 atoms. Because of its size, for this work, local shape of the energy surface along the transition path was not determined and the entropy assumed constant.

There were performed and compared two series of calculations in which the molecule position was advanced differently. Either single carbon atom or the whole molecule had the considered coordinate updated. Preliminary checks have shown that this difference has no effect on the numerical results and computing time required.

As the molecule was pulled across the surface rows, it rotated to avoid breaking the O-In bonds. The abrupt energy drops visible at about 2.5 Å and 5.5 Å on the Fig. 3.11 are artifacts of the method used and correspond to discontinuous movement of the molecule as it departs form a top of en-

Figure 3.11: Energy of the PTCDA/InSb(001) system along the path of simulated diffusion across the surface rows ($[1\bar{1}0]$). The horizontal axis shows the travelled distance in Å and the dashed vertical lines are spaced by one LEED unit. The yellow line corresponds to half of the length of the simulation cell and to a quarter of the length of the true $c(8 \times 2)$ reconstruction cell.
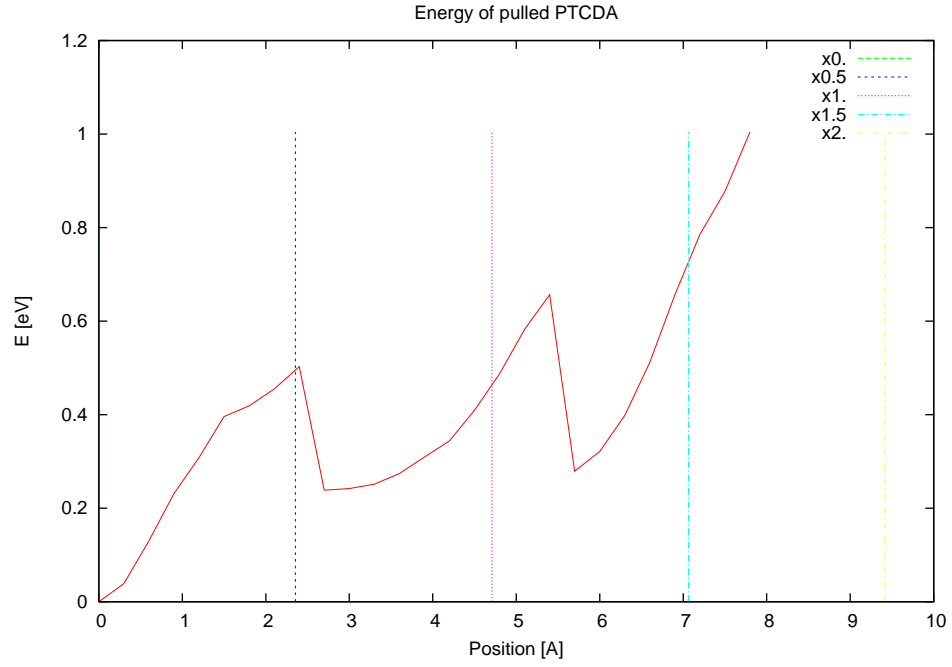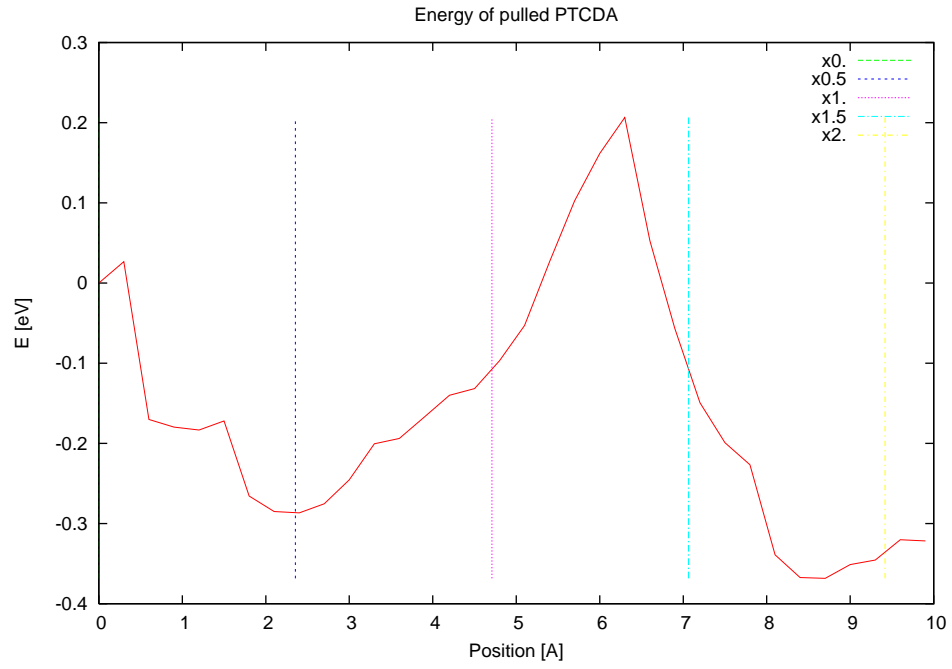
Figure 3.12: Energy of the PTCDA/InSb(001) system along the path of simulated diffusion along the surface rows ([110]). The horizontal axis shows the travelled distance in Å and the dashed vertical lines are spaced by one LEED unit. The yellow line corresponds to the width of the $c(8 \times 2)$ reconstruction cell.

ergy barrier. These barriers are of about 0.5 eV and are accessible in room temperature. However, as the final points of the plot show, a barrier of more than 1 eV is encountered as the molecule. It makes further movement of PTCDA in this direction impossible.

Diffusion in the other direction, along the surface rows, is found to be also complex, but not hindered by high barriers. Since the substrate has periodic structure, we could expect that energy of a molecule pushed over it would change periodically too. Still, results of the procedure performed here do not repeat as the whole width of the reconstruction cell is traversed. This behaviour is caused be an additional indium atom pulled behind the molecule. The starting geometry of the system used in this simulation is the low energy case shown in the Table 3.1 as $\alpha_0 = 90°$, $x_0 = 1$, $y_0 = 1$. The case $\alpha_0 = 90°$, $x_0 = 1$, $y_0 = 0.5$ has even more favourable binding energy, but it was not known at the time the diffusion simulation was started. This fact manifests itself as the energy minimum on the plot located at 0.5 LEED distance (blue vertical line). The discontinuities on the plot correspond to switching of the chemical bonds of oxygen and indium. To illustrate this, two subsequent frames of the simulation, that embrace the event are presented in Fig. 3.13.

The energy maximum visible on the plot (Fig. 3.12) delimit the energy barriers that the diffusing molecule has to overcome. They are about 0.5 eV at most, hence we conclude that in room temperature the molecule can move along the rows, in the [110] direction. These barriers are so low, because the
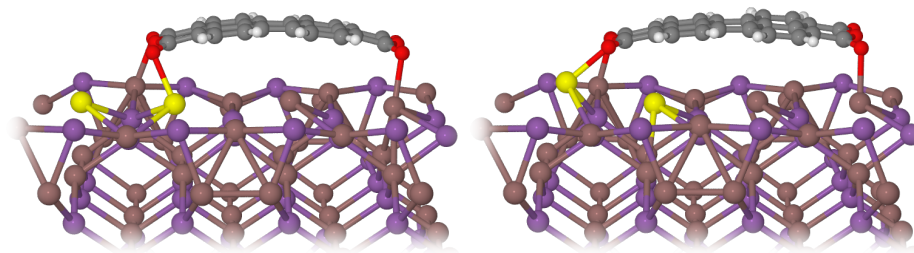
Figure 3.13: Two consecutive optimal configurations taken from the diffusion calculation. Two indium atoms involved in the bond switching are represented as yellow spheres.

four chemical bonds, in which the molecule is involved, are not simultaneously broken, but the indium atoms are exchanged one by one instead.

A particularly low energy configuration which gives rise to the minimum seen at 8.5 Å on Fig. 3.12 was discovered. Two of the indium atoms, which originally occupy the In-1 sites, being involved in the O-In bonds in this structure are significantly displaced and seemingly bonded together. After the clustering of surface indium atoms was studied, it is now understood that the proximity of these two indium atoms causes the energy gain observed.

3.8 Interaction with In-1 atoms

When seeking for theoretical predictions about a system like PTCDA adsorbed on crystal surface or about the reconstructed surface alone, the following two problems can be formulated: how the system behaves locally, what possible geometries of unit cell correspond to low energies, and what is its global behaviour, how often these particular local structures should be

88
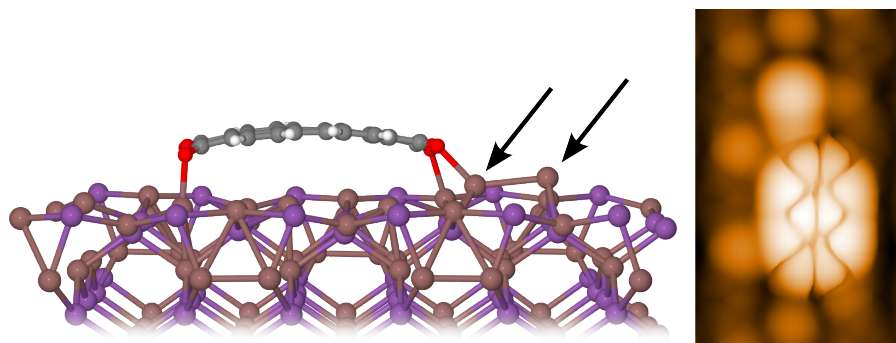
Figure 3.14: PTCDA adsorbed on the surface with an additional indium atom elevated (right arrow) to form a bond with the In atom involved in the O-In bond (left arrow). An optimized geometry (left) and a corresponding simulated STM image for -1 V bias voltage (right).

encountered.

The global finite temperature properties of InSb(001) $c(8 \times 2)$ surface are governed by small energy differences and cannot be reproduced by DFT calculations employed in this work. Similar difficulties prevent complete treatment of the PTCDA/InSb problem.

As was discussed before, a particularly preferable arrangement of In-1 atoms close to the molecule is obtained if one In-1 atom is moved close to the In-1 atom bound to oxygen, so that an extra dimer is formed (Fig. 3.14). This change lowers the total energy by about 0.1 eV. Figure 3.14 (right part) is a simulated STM image of occupied states of this new system. It demonstrates that the lifted atom appears as a bright spot next to the image of PTCDA. It is located on the In-1 row, so it is closer to the the less pronounced half of PTCDA image.

Such bright spots are indeed observed in STM images at ends of molecular

chains (Fig. 3.8 a, c). As can be seen on Fig. 3.8c, these extra spots are located near the smaller oval of image of the last molecule in the chain. In this case the agreement between experiment and simulation is excellent.

Once we understand the nature of these bright spots, an important question is raised: can chain assembly be hindered by presence of these elevated indium atoms?

For this, a transition between two states was studied by series of simple constrained optimizations, as discussed in Section 1.4.1. The arrangement with dimer with elevated indium atom was chosen as the initial state (Fig. 3.14). This atom was pushed towards the next In-1 site, which was initially unoccupied. Evolution of system energy is shown on Fig. 3.15.

As expected, the energy grows. The barrier which the pulled away atoms has to overcome is 0.2 eV. The reverse transition requires half of this energy. It means that the elevated indium atoms are able to recede to nearest vacant In-1 site. It should be noted that in this case it remains unknown how much these barriers are affected by entropic effects.

As discussed before, the atoms labelled In-1 are mobile. Also, there about two vacancies per every five In-1 sites. The problem of energetically most favourable arrangements of these atoms on pure InSb surface was mostly solved. However, this knowledge is not very helpful when seeking for best geometries with PTCDA molecule involved. This is because the strong interaction of In-1 atoms and the molecule distorts formation of the dimers or trimers discussed in section 2.4.
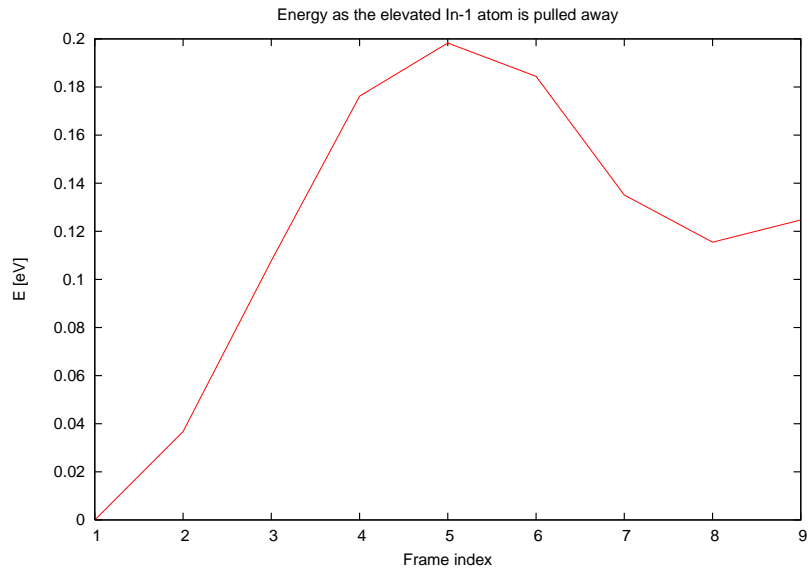
Figure 3.15: Energy of the PTCDA/InSb system in which the elevated indium atom (Fig. 3.14) is pushed down to the In-1 site along the [110] direction.

Several cases of PTCDA adsorbed on the surface with In-1 vacancies were studied. It was found that whenever there are four indium atoms available close to the molecule, four covalent O-In bonds are formed the same way as previous calculations unveiled. In these cases adsorption energies are also similar to those previously found. If location of the vacancies prevents formation of one of these bonds, the binding energy is lower by approximately 0.4 eV. Because coverages of PTCDA considered in this work are low, we can assume that there is always an indium atom available that can move along the In-1 row to form the energetically favourable chemical bond. We can conclude that thorough examination of the many possible arrangements of PTCDA on surface with lower In-1 occupancy would not bring any new insight.

Summary

The work presented in this thesis is concerned with atomic and molecular structures on a crystal surface and their theoretical treatment by means of density functional theory calculations. The surface science and nanotechnology meets computational physics in this work.

The first chapter explains how the problem of many electrons in the potential of atomic nuclei is solved. It also highlights the problems and algorithms of exploration of the phase space of classical motion of the atoms. Next, justification of density functional theory is presented and its essence is explained. These techniques were then employed to deliver the results discussed in the remaining chapters.

In particular, a complicated reconstruction of indium-rich InSb and InAs surfaces is studied. It is known from experiments that $c(8 \times 2)$ and 4×2 symmetries are present on these surfaces. However, STM observations also reveal that at low temperatures this order is broken and the acquired images feature complicated patterns. Their nature was initially not understood.

The mystery was solved as calculations, presented in the second chapter,

indicated that clustered structures of the In-1 atoms have lower energies than the corresponding, initially assumed model arrangement. It was also discovered that the their movement along these rows does not require large energies, so that they are mobile in room temperature.

The indium cluster structures described here are observed in low temperatures and not visible above 180 K. Therefore an interesting question arises, namely whether they undergo a phase transition. The issue is complicated by the fact that these different structures in various environments enjoy very different stability. Hence we cannot expect to find a single particular temperature corresponding to the transition in general.

Let us note another interesting fact, that the traces left by the fluctuations of the In-1 row in the STM images observed at room temperature are very unspecific. There appears a smooth line along the outstanding indium row, so that the first model considered in this work, with all the In-1 sites occupied, seems sufficient.

To summarize, the combined experimental and theoretical results discussed here, lead to a model of the indium-rich InSb(001) and InAs (001) surfaces that is similar to the model ζ proposed by Kumpf et al., but the indium atoms in its dominant rows form clustered structures. The base model ζ served as a starting point and computations have shown that it is stable, but with higher total energy.

In the third chapter calculations and findings about PTCDA adsorbed on the InSb surface are discussed. Several configurations featuring the highest

binding energy are found. Bound molecules are no longer flat and the available energy permits significant bending of its perylene core. Calculations reveal also that in this system a charge of more than $2e$ is transferred.

Several simulated STM images were presented in this thesis. In general, they all are in agreement with experimental observations. We are able to recognize corresponding features on the images. Most prominently, the PTCDA molecule exhibits many details which have close resemblance to the ones found in the real scan results. This consistency suffices so that the way the molecule adsorbs to the surface can be unequivocally stated. Moreover, we attain understanding of the role played by the covalent bods formed between oxygen atoms of the molecule and surface indium atoms. It is shown that they constrain movements of the molecule to the direction of outstanding surface rows. Interestingly, the four bonds the molecule forms with the surface act as four legs: they can move forward to next lattice sites one by one. The above facts can serve as a basis for possible explanation why the molecules form chains on the surface. We are only missing the intermolecular attraction to be elucidated. It would give us complete picture of the considered system.

Some of the results of calculations performed for this work are published together with corresponding experimental studies in the papers [i], [ii], [iii] and [iv].

It should be said that thanks to the experimental efforts and the results made available to help the work presented here, it was possible to perform

these calculations in a well focused manner. This interaction helped to make them satisfactory and conclusive. Hopefully, not only the results and conclusions can be helpful for related future work, but also the reasoning and methods found here can suggest new solutions in related areas of nanotechnology and surface science.

Bibliography

[1] C. Joachim, J. K. Gimzewski, and A. Aviram, "Electronics using hybrid-molecular and mono-molecular devices," *Nature*, vol. 408, no. 6812, pp. 541–548, 2000. 10.1038/35046000.

[2] B. Silvi and A. Savin, "Classification of chemical bonds based on topological analysis of electron localization functions," *Nature*, vol. 371, no. 6499, pp. 683–686, 1994. 10.1038/371683a0.

[3] S. Goedecker, "Minima hopping: An efficient search method for the global minimum of the potential energy surface of complex molecular systems," *The Journal of Chemical Physics*, vol. 120, no. 21, pp. 9911–9917, 2004.

[4] J. Nocedal, "Updating quasi-Newton matrices with limited storage," *Math. Comp.*, vol. 35, pp. 773–782, Jul 1980.

[5] M. R. Hestenes and E. Stiefel, "Methods of conjugate gradients for solving linear systems," *Journal of Research of the National Bureau of Standards*, vol. 49, pp. 409–436, Dec 1952.

[6] E. Bitzek, P. Koskinen, F. Gähler, M. Moseler, and P. Gumbsch, "Structural relaxation made simple," *Phys. Rev. Lett.*, vol. 97, p. 170201, Oct 2006.

[7] S. Kirkpatrick, C. D. Gelatt, and M. P. Vecchi, "Optimization by simulated annealing," *Science*, vol. 220, no. 4598, pp. 671–680, 1983.

[8] S. A. Trygubenko and D. J. Wales, "A doubly nudged elastic band method for finding transition states," *The Journal of Chemical Physics*, vol. 120, no. 5, pp. 2082–2094, 2004.

[9] W. M. C. Foulkes, L. Mitas, R. J. Needs, and G. Rajagopal, "Quantum monte carlo simulations of solids," *Rev. Mod. Phys.*, vol. 73, pp. 33–83, Jan 2001.

[10] J. B. Anderson, "A random-walk simulation of the schrödinger equation: H_3^+," *The Journal of Chemical Physics*, vol. 63, no. 4, pp. 1499–1503, 1975.

[11] J. B. Anderson, "Quantum chemistry by random walk: Higher accuracy," *The Journal of Chemical Physics*, vol. 73, no. 8, pp. 3897–3899, 1980.

[12] J. B. Anderson, "Quantum chemistry by random walk. H ^{2}P, H_3^+ D_{3h} ^{1}A'$_1$, H_2 $^3\sigma_u^+$, H_4 $^1\sigma_g^+$, Be ^{1}S," *The Journal of Chemical Physics*, vol. 65, no. 10, pp. 4121–4127, 1976.

[13] V. Fock, "Näherungsmethode zur lösung des quantenmechanischen mehrkörperproblems," *Zeitschrift für Physik A Hadrons and Nuclei*, vol. 61, pp. 126–148, 1930. 10.1007/BF01340294.

[14] J. C. Slater, "A simplification of the Hartree-Fock method," *Phys. Rev.*, vol. 81, pp. 385–390, Feb 1951.

[15] C. D. Sherrill and H. F. S. III, "The configuration interaction method: Advances in highly correlated approaches," vol. 34 of *Advances in Quantum Chemistry*, pp. 143 – 269, Academic Press, 1999.

[16] R. J. Bartlett, "Many-body perturbation theory and coupled cluster theory for electron correlation in molecules," *Annual Review of Physical Chemistry*, vol. 32, no. 1, pp. 359–401, 1981.

[17] R. J. Bartlett and M. Musiał, "Coupled-cluster theory in quantum chemistry," *Rev. Mod. Phys.*, vol. 79, pp. 291–352, Feb 2007.

[18] P.-O. Löwdin, "Quantum theory of many-particle systems. i. physical interpretations by means of density matrices, natural spin-orbitals, and convergence problems in the method of configurational interaction," *Phys. Rev.*, vol. 97, pp. 1474–1489, Mar 1955.

[19] Y.-K. Liu, M. Christandl, and F. Verstraete, "Quantum computational complexity of the n-representability problem: QMA complete," *Phys. Rev. Lett.*, vol. 98, p. 110503, Mar 2007.

[20] D. A. Mazziotti, "Parametrization of the two-electron reduced density matrix for its direct calculation without the many-electron wave function," *Phys. Rev. Lett.*, vol. 101, p. 253002, Dec 2008.

[21] A.M.K. and Müller, "Explicit approximate relation between reduced two- and one-particle density matrices," *Physics Letters A*, vol. 105, no. 9, pp. 446 – 452, 1984.

[22] M. A. Buijse and E. J. Baerends, "An approximate exchange-correlation hole density as a functional of the natural orbitals," *Molecular Physics*, vol. 100, no. 4, pp. 401–421, 2002.

[23] M. Levy, "Universal variational functionals of electron densities, first-order density matrices, and natural spin-orbitals and solution of the *v*-representability problem," *Proceedings of the National Academy of Sciences*, vol. 76, no. 12, pp. 6062–6065, 1979.

[24] P. Hohenberg and W. Kohn, "Inhomogeneous electron gas," *Phys. Rev.*, vol. 136, pp. B864–B871, Nov 1964.

[25] T. Kato, "On the eigenfunctions of many-particle systems in quantum mechanics," *Communications on Pure and Applied Mathematics*, vol. 10, no. 2, pp. 151–177, 1957.

[26] T. L. Gilbert, "Hohenberg-Kohn theorem for nonlocal external potentials," *Phys. Rev. B*, vol. 12, pp. 2111–2120, Sep 1975.

[27] J. E. Harriman, "Orthonormal orbitals for the representation of an arbitrary density," *Phys. Rev. A*, vol. 24, pp. 680–682, Aug 1981.

[28] H. Chen and A. Zhou, "Orbital-free density functional theory for molecular structure calculations," *Numerical Mathematics: Theory, Methods and Applications*, vol. 1, pp. 1–28, Nov 2007.

[29] Péter and Pulay, "Convergence acceleration of iterative sequences. the case of SCF iteration," *Chemical Physics Letters*, vol. 73, no. 2, pp. 393 – 398, 1980.

[30] C. Fiolhais, "A primer in density functional theory," *Materials Today*, vol. 6, no. 12, p. 59, 2003.

[31] O. Gunnarsson and B. I. Lundqvist, "Exchange and correlation in atoms, molecules, and solids by the spin-density-functional formalism," *Phys. Rev. B*, vol. 13, pp. 4274–4298, May 1976.

[32] J. P. Perdew and Y. Wang, "Accurate and simple analytic representation of the electron-gas correlation energy," *Phys. Rev. B*, vol. 45, pp. 13244–13249, Jun 1992.

[33] J. P. Perdew, K. Burke, and M. Ernzerhof, "Generalized gradient approximation made simple," *Phys. Rev. Lett.*, vol. 77, pp. 3865–3868, Oct 1996.

[34] H. J. Monkhorst and J. D. Pack, "Special points for Brillouin-zone integrations," *Phys. Rev. B*, pp. 5188–5192, 1976.

[35] G. Binnig, H. Rohrer, C. Gerber, and E. Weibel, "Surface studies by scanning tunneling microscopy," *Phys. Rev. Lett.*, vol. 49, pp. 57–61, Jul 1982.

[36] J. Tersoff and D. R. Hamann, "Theory of the scanning tunneling microscope," *Phys. Rev. B*, vol. 31, pp. 805–813, Jan 1985.

[37] J. Bardeen, "Tunnelling from a many-particle point of view," *Phys. Rev. Lett.*, vol. 6, pp. 57–59, Jan 1961.

[38] J. M. Soler, E. Artacho, J. D. Gale, A. García, J. Junquera, P. Ordejón, and D. Sánchez-Portal, "The SIESTA method for ab initio order-N materials simulation," *Journal of Physics: Condensed Matter*, vol. 14, no. 11, p. 2745, 2002.

[39] P. Ordejón, E. Artacho, and J. M. Soler, "Self-consistent order-N density-functional calculations for very large systems," *Phys. Rev. B*, vol. 53, pp. R10441–R10444, Apr 1996.

[40] J. VandeVondele, M. Krack, F. Mohamed, M. Parrinello, T. Chassaing, and J. Hutter, "Quickstep: Fast and accurate density functional calculations using a mixed gaussian and plane waves approach," *Computer Physics Communications*, vol. 167, no. 2, pp. 103–128, 2005.

[41] J. VandeVondele and J. Hutter, "An efficient orbital transformation method for electronic structure calculations," *The Journal of Chemical Physics*, vol. 118, no. 10, pp. 4365–4369, 2003.

[42] G. Kresse and J. Hafner, "Ab initio molecular dynamics for liquid metals," *Phys. Rev. B*, vol. 47, pp. 558–561, Jan 1993.

[43] G. Kresse and J. Hafner, "Ab initio molecular-dynamics simulation of the liquid-metal–amorphous-semiconductor transition in germanium," *Phys. Rev. B*, vol. 49, pp. 14251–14269, May 1994.

[44] G. Kresse and J. Furthmüller, "Efficiency of ab-initio total energy calculations for metals and semiconductors using a plane-wave basis set," *Computational Materials Science*, vol. 6, no. 1, pp. 15–50, 1996.

[45] G. Kresse and J. Furthmüller, "Efficient iterative schemes for ab initio total-energy calculations using a plane-wave basis set," *Phys. Rev. B*, vol. 54, pp. 11169–11186, Oct 1996.

[46] Q.-K. Xue, T. Hashizume, and T. Sakurai, "Scanning tunneling microscopy of III-V compound semiconductor (001) surfaces," *Progress in Surface Science*, vol. 56, no. 1-2, pp. 1 – 131, 1997.

[47] Q. Xue, T. Hashizume, J. M. Zhou, T. Sakata, T. Ohno, and T. Sakurai, "Structures of the Ga-rich 4×2 and 4×6 reconstructions of the GaAs(001) surface," *Phys. Rev. Lett.*, vol. 74, pp. 3177–3180, Apr 1995.

[48] C. F. McConville, T. S. Jones, F. M. Leibsle, S. M. Driver, T. C. Q. Noakes, M. O. Schweitzer, and N. V. Richardson, "Surface reconstructions of InSb(100) observed by scanning tunneling microscopy," *Phys. Rev. B*, vol. 50, pp. 14965–14976, Nov 1994.

[49] G. Goryl, D. Toton, N. Tomaszewska, J. S. Prauzner-Bechcicki, L. Walczak, A. Tejeda, A. Taleb-Ibrahimi, L. Kantorovich, E. G. Michel, and J. J. Kolodziej, "Structure of the indium-rich InSb(001) surface," *Phys. Rev. B*, vol. 82, p. 165311, Oct 2010.

[50] G. Goryl, O. Boelling, S. Godlewski, J. Kolodziej, B. Such, and M. Szymonski, "Low temperature insb(001) surface structure studied by scanning tunneling microscopy," *Surface Science*, vol. 601, no. 17, pp. 3605 – 3610, 2007.

[51] P. John, T. Miller, and T.-C. Chiang, "InSb(100) reconstructions probed with core-level photoemission," *Phys. Rev. B*, vol. 39, pp. 1730–1737, Jan 1989.

[52] D. K. Biegelsen, R. D. Bringans, J. E. Northrup, and L.-E. Swartz, "Surface reconstructions of GaAs(100) observed by scanning tunneling microscopy," *Phys. Rev. B*, vol. 41, pp. 5701–5706, Mar 1990.

[53] S.-H. Lee, W. Moritz, and M. Scheffler, "GaAs(001) surface under conditions of low as pressure: Evidence for a novel surface geometry," *Phys. Rev. Lett.*, vol. 85, pp. 3890–3893, Oct 2000.

[54] C. Kumpf, D. Smilgies, E. Landemark, M. Nielsen, R. Feidenhans'l, O. Bunk, J. H. Zeysing, Y. Su, R. L. Johnson, L. Cao, J. Zegenhagen, B. O. Fimland, L. D. Marks, and D. Ellis, "Structure of metal-rich (001)

surfaces of III-V compound semiconductors," *Phys. Rev. B*, vol. 64, p. 075307, Jul 2001.

[55] S. García-Gil, A. García, N. Lorente, and P. Ordejón, "Optimal strictly localized basis sets for noble metal surfaces," *Phys. Rev. B*, vol. 79, p. 075441, Feb 2009.

[56] G. Goryl, D. Toton, M. Goryl, N. Tomaszewska, and J. Kolodziej, "Structure of the In-rich InAs (001) surface," *Surface Science*, vol. 605, no. 23-24, pp. 2073 – 2081, 2011.

[57] D. Toton, J. He, G. Goryl, J. J. Kolodziej, S. Godlewski, L. Kantorovich, and M. Szymonski, "Structure of InSb(001) surface," *Journal of Physics: Condensed Matter*, vol. 22, no. 26, p. 265001, 2010.

[58] Y. Hirose, A. Kahn, V. Aristov, P. Soukiassian, V. Bulovic, and S. R. Forrest, "Chemistry and electronic properties of metal-organic semiconductor interfaces: Al, Ti, In, Sn, Ag, and Au on PTCDA," *Phys. Rev. B*, vol. 54, pp. 13748–13758, Nov 1996.

[59] S. Boys and F. Bernardi, "The calculation of small molecular interactions by the differences of separate total energies. some procedures with reduced errors," *Molecular Physics*, vol. 19, no. 4, pp. 553–566, 1970.

[60] F. B. van Duijneveldt, J. G. C. M. van Duijneveldt-van de Rijdt, and J. H. van Lenthe, "State of the art in counterpoise theory," *Chemical Reviews*, vol. 94, no. 7, pp. 1873–1885, 1994.

[61] S. Godlewski, G. Goryl, A. Gourdon, J. J. Kolodziej, B. Such, and M. Szymonski, "Internal architecture and adsorption sites of Violet Lander molecules assembled on native and KBr-passivated InSb(001) surfaces," *ChemPhysChem*, vol. 10, no. 12, pp. 2026–2033, 2009.

[62] D. Toton, S. Godlewski, G. Goryl, J. J. Kolodziej, L. Kantorovich, and M. Szymonski, "Architecture of PTCDA molecular structures on a reconstructed InSb(001) surface," *Phys. Rev. B*, vol. 83, p. 235431, Jun 2011.

[63] L. Romaner, D. Nabok, P. Puschnig, E. Zojer, and C. Ambrosch-Draxl, "Theoretical study of PTCDA adsorbed on the coinage metal surfaces, Ag(111), Au(111) and Cu(111)," *New Journal of Physics*, vol. 11, no. 5, p. 053010, 2009.

[64] L. Romaner, G. Heimel, J.-L. Brédas, A. Gerlach, F. Schreiber, R. L. Johnson, J. Zegenhagen, S. Duhm, N. Koch, and E. Zojer, "Impact of bidirectional charge transfer and molecular distortions on the electronic structure of a metal-organic interface," *Phys. Rev. Lett.*, vol. 99, p. 256801, Dec 2007.

[65] A. Hauschild, K. Karki, B. C. C. Cowie, M. Rohlfing, F. S. Tautz, and M. Sokolowski, "Molecular distortions and chemical bonding of a large π-conjugated molecule on a metal surface," *Phys. Rev. Lett.*, vol. 94, p. 036106, Jan 2005.

[i]   G. Goryl, D. Toton, N. Tomaszewska, J. S. Prauzner-Bechcicki, L. Wal-
        czak, A. Tejeda, A. Taleb-Ibrahimi, L. Kantorovich, E. G. Michel, and
        J. J. Kolodziej, "Structure of the indium-rich InSb(001) surface," *Phys.
        Rev. B*, vol. 82, p. 165311, Oct 2010.

[ii]   D. Toton, J. He, G. Goryl, J. J. Kolodziej, S. Godlewski, L. Kantorovich,
        and M. Szymonski, "Structure of InSb(001) surface," *Journal of Physics:
        Condensed Matter*, vol. 22, no. 26, p. 265001, 2010.

[iii]   D. Toton, S. Godlewski, G. Goryl, J. J. Kolodziej, L. Kantorovich, and
        M. Szymonski, "Architecture of PTCDA molecular structures on a re-
        constructed InSb(001) surface," *Phys. Rev. B*, vol. 83, p. 235431, Jun
        2011.

[iv]   G. Goryl, D. Toton, M. Goryl, N. Tomaszewska, and J. Kolodziej, "Struc-
        ture of the In-rich InAs (001) surface," *Surface Science*, vol. 605, no. 23-
        24, pp. 2073 – 2081, 2011.